Nanomedicine

Design of polymeric nanocapsules to improve their lympho-targeting capacity

Journal:	*Nanomedicine*
Manuscript ID	Draft
Manuscript Type:	Research Article
Keywords:	inulin, chitosan, nanocapsules, particle size, Targeting, Dendritic cells, lymph nodes, 2-Photon microscopy

SCHOLARONE™
Manuscripts

Abstract

Aim: To design lympho-targeted nanocarriers for enhancing the activity of associated drugs/antigens whose target is within the lymphatic system. **Materials & Methods**: inulin-based NCs, negatively charged, and positively charged chitosan NCs were prepared by the solvent displacement techniques. The NCs were produced in two sizes: small (≈ 70 nm) and medium (170 – 250 nm). **Results:** *In vitro* results indicated that the small NCs interacted more with dendritic cells. The study of the NCs biodistribution in mice, using 3D reconstruction of the popliteal lymph node, showed the highest accumulation for small inulin NCs. These NCs exhibited the greatest interaction with all the subsets of resident immune cells. **Conclusion:** small inulin NCs confirmed their foreseen lympho-targeting properties.

Graphical abstract:

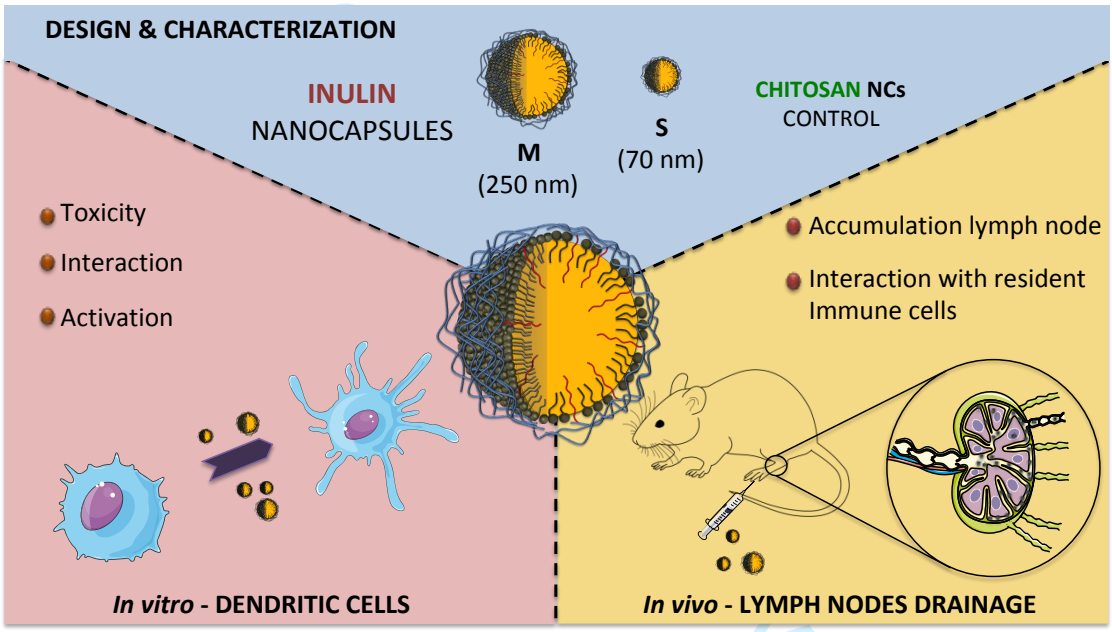

Keywords: Inulin; chitosan; nanocapsules; particle size; targeting; dendritic cells; lymph nodes; 2-photon microscopy

1. Introduction

Polysaccharides are excellent biomaterials for the design of antigen/drug delivery carriers [1]. Among them, inulin (INU), composed by polyfructose chains with a terminal glucose, has been used in the food and pharmaceutical industry as a stabilizing agent and has a GRAS status [2]. In vaccination, INU microparticles have shown to enhance humoral and cellular immune responses against different antigens [3]. Advax™, composed by delta-INU in microcrystalline form, has been tested in combination with different antigens in clinical trials, including HIV and influenza (phase I), and hepatitis and allergy (phase II) vaccines [4,5]. The particle size of Advax™ (1-2 μm) and its low solubility favor a depot effect when injected either subcutaneously or intramuscularly. Then, the immune cells engulf the microparticles and transport them to secondary lymphoid organs [6].

Considering the ability of macrophages and dendritic cells (DCs) to uptake lymph-borne antigens and initiate the innate and adaptive immune responses [7], researchers have hypothesized that lympho-targeted antigen nanocarriers would be beneficial, as compared to the classical depot microparticles, in terms of making more direct and effective their access to these immune cells. This increasingly evident hypothesis is changing the paradigm of nanovaccine design, with more and more nanosystems being engineered to have an efficient drainage to the lymphatics [8–12]. In this context, it is commonly agreed that a value of 100 nm is the threshold below which nanoparticles (NPs) may drain relatively easily along the lymphatic vessels [13–15]. Recent research in this field, specially oriented to cancer vaccines, has led to the development of different types of nanocarriers with lympho-targeting properties, such as silica [16] and gold NPs [17], micelles [18], poly(propylene sulfide) NPs [19], polystyrene NPs [20] and liposomes [21], among others [8]. However, the majority of these nanosystems are model NPs and/or have a questionable translational potential.

Interestingly, despite the long trajectory of INU as a pharmaceutical excipient, as well as microparticulated antigen delivery system, its use as a biomaterial in the design of nanovaccines has been, so far, barely explored [22].

Therefore, bearing this background information in mind, the first objective of this study was to develop INU NCs and to characterize them with regard to their morphology and physicochemical properties.

The second goal of this work was to perform a systematic study of the influence of the composition and physicochemical properties of polymeric NCs on their interaction with DCs, and also on their biodistribution. Overall, our ultimate goal has been to contribute to the rational design of new nanovaccines to maximize their specific drainage to the lymphatic system and to elicit a directly controlled immune response.

For Review Only

2. Materials & Methods

2.1. Materials

DL-α-tocopherol (vitamin E) (Calbiochem®) was obtained from Merck Millipore (Billerica, MA, USA) and Pluronic® 127 (Poloxamer 407) from BASF (Ludwigshafen, Germany). Sodium glycocholate was bought to Dextra (Reading, UK). Benzethonium chloride was obtained from Spectrum Chemical Mgf. Corp. (NJ, US). Ultrapure chitosan (CS) hydrochloride salt (Mw 42.7 kDa, deacetylation degree of 88%) was purchased from Heppe Medical Chitosan GmbH (Saale, Germany). Inutec® SL1 (25% modified inulin suspension in glycerol) was a kind gift from CreaChem (Tienen, Belgium). 1,1'-dioctadecyl-3,3,3',3'-tetramethylindodicarbocyanine perchlorate (DiD) was obtained from Invitrogen (CA, USA) and sucrose was purchased from Acofarma (Madrid, Spain)

All other chemicals were of reagent grade or high purity. For *in vitro* and *in vivo* experiments endotoxin free water and sterile/autoclaved material were used.

2.2. Preparation of the nanosystems

2.2.1. Screening of different ratios inulin:vitamin E and incorporation of co-surfactants

NCs were prepared by the solvent displacement technique [23]. Briefly, 60 mg of vitamin E dissolved in 2 mL of ethanol were poured over 4 mL of an aqueous solution of Inutec® SL1 (60 mg, 30 mg and 15 mg, for a ratio Inutec®:vitamin E of 1:1, 0.5:1 and 0.25:1, respectively). The addition was performed under stirring that was kept for 10 minutes before characterization of the nanosystems. In the case of NCs containing a co-surfactant, sodium glycocholate or benzethonium chloride, this was added in the ethanolic phase as an aqueous solution (50 µL of sodium glycocholate 200 mg/mL or 100 µL of benzethonium chloride 20 mg/mL).

2.2.2. Preparation of medium (M) and small (S) size chitosan and inulin nanocapsules

The NCs were prepared following a similar protocol than the one described in section 2.2.1. The vitamin E was dissolved in ethanol (**Table 1**) and the glycocholate was added to this phase as a 200 mg/mL aqueous solution. The polymers (CS or INU) were added to the aqueous phase. For CS NCs poloxamer 407 was used as surfactant in the aqueous phase. The different amounts of compounds and solvents are shown in **Table 1**. To obtain the S NCs the organic phase was injected into the aqueous phase through a needle (100 Sterican®, Ø 0.60 x 60 mm, 23G x $2^{3/8}$", Braun, Melsungen, Germany) applying high manual pressure (approximately, a flow of 2 mL/s). In both cases, the aqueous phase was maintained under stirring during the

For Review Only

addition. After 10 minutes of incubation, the excess of ethanol was removed under vacuum using a rotary evaporator (Büchi, Switzerland), and the volume adjusted with ultrapure water.

Table 1. Different composition and preparation parameters of the nanosystems developed in this study.

	INU NCs S	**INU NCs M**	**CS NCs S**	**CS NCs M**
Vitamin E (mg)	30	60	30	60
Sodium glycocholate (mg)	5	10	5	10
Ethanol (mL)	2.5	2	2.5	3
Poloxamer 407 (mg)	-	-	5	10
Chitosan (mg)	-	-	5	10
Inutec® SL1 (mg)	15	30	-	-
Water (mL)	10	4	10	4
Stirring speed (rpm)	*900*	*500*	*900*	*500*
Addition	*High pressure (injecting)*	*Low pressure (pouring)*	*High pressure (injecting)*	*Low pressure (pouring)*
Final volume (mL)	*5*	*10*	*5*	*10*
Final concentration (mg/mL)	*10*	*10*	*9*	*9*

2.2.3. Labeled nanocapsules

For *in vitro* and *in vivo* studies, the NCs were labeled with the fluorescent marker DiD. For that purpose, DiD-loaded NCs were obtained by replacing the same amount of ethanol with the required amount of an ethanolic solution of DiD 2.5 mg/mL. The theoretical final concentration of DiD went from 10 to 100 µg/mL, depending on the experiment.

2.3. Physicochemical characterization

Particle size, polydispersity index, and zeta-potential were measured by photon correlation spectroscopy using a Zetasizer Nano-S (Malvern Instruments; Malvern, UK). The S NCs were diluted 1:10 and M NCs 1:20 in water prior to their measurement. Analyses were performed at 25 ºC with a detection angle of 173 º in distilled water.

The pH of the formulations was determined with a Sartorius Docu-pH Benchtop Meter (Thermo Fisher Scientific, Waltham, MA, USA).

2.3.1. Electron microscopy studies

The morphology of the NCs was examined by different electron microscopy techniques:

- *Transmission electron microscopy (TEM)*

For Review Only

For the negative staining a 4 µL drop of each sample was left to dry for 15 min on a 200-mesh copper grid covered with a formvar-carbon film. Then, the excess liquid was removed with a filter paper, serially washed with three drops of ultrapure water, followed by incubation during 30 s with a drop of 1% uranyl acetate solution. Afterwards, the excess of uranyl solution was removed with a filter paper and the grids were left to dry before observing them in the microscope (Thermo-Fisher (MA, USA) Tecnai G2 20 Twin) operating at 120 kV.

- *Sample vitrification and Cryo-TEM*

For Cryo-TEM visualization, samples were vitrified putting 4 µL of the NCs solution over a previously glow-discharged Quantifoil R2/2 200-mesh copper grid and using a Vitrobot Mark IV (Thermo-Fisher (MA, USA)). Grids were observed in the TEM under cryo-conditions, mounting the grids on a GATAN 626 cryo-holder, and operating at 120 kV under low-dose conditions.

- *Field emission scanning electron microscopy (FESEM)*

For FESEM studies (ZEISS FESEM ULTRA Plus, Germany) the NCs were diluted in water 1:1000 and mixed with the same volume of 2% (w/v) phosphotungstic acid solution. 1 µL of this mixture was placed on copper grids with carbon films. The grids were left to dry in the open air and then washed drop-by-drop with 1 mL of water. Once the grids were dried they were observed in the microscope using both STEM and InLens detectors.

2.3.2. Nanoparticle tracking Analysis

Nanoparticle tracking analysis (NTA) is a method to measure the particle size of NPs based on imaging. The light scattered for individual NPs is captured by a camera. The software (v3.3) uses the Stokes-Einstein equation to transform the Brownian movement into a particle size. The experiments were conducted after diluting the NCs (1:2000) in ultrapure water (MilliQ®) using a NanoSight NS3000 equipment (Malvern Panalytical Ldt, UK). Five videos of each sample were captured over 90 s, maintaining the temperature stable at 25 ºC. All measurements were performed in triplicate.

2.4. Freeze-drying studies

NCs were freeze-dried in the presence of sucrose as cryoprotectant at different final concentrations (10 and 15% (w/v)). NCs and sugar solution were mixed 1:1 (v/v) to 1 mL in a 5 mL freeze-drying glass vials. Vials were quickly frozen at -80 ºC and then transferred to the freeze-drier Genesis 25 ES, VirTis Model-Wizard 2.0 (SP Industries, USA). The primary drying lasted for 35 h with temperatures increasing from -40 to -20 ºC. In the secondary drying step, the temperature of the samples was raised gradually up to +20 ºC.

For Review Only

2.5. Colloidal stability

2.5.1. Stability at storage conditions

Suspensions of the different NCs were stored at 4 ºC for 1 month. At fixed time points their size, PDI, and zeta-potential were determined, as described in section 2.4.

2.5.2 Stability in cell culture media

The stability of the NCs diluted 1:10 in cell culture medium (RPMI supplemented with 10% fetal bovine serum (FBS)) at 37 ºC was followed for up to 24 h, and the evolution of particle size and PDI was carefully monitored.

2.6. Human Dendritic Cell generation

Human peripheral blood mononuclear cells (PBMCs) were obtained by anonymous donors. Studies were approved by the ethical committee of the Xunta de Galicia (register code 2014/543). PBMCs were isolated by Ficoll centrifugation. Adherent monocytes were isolated by incubation of PBMCs in culture plates (2 h, 37 ºC) in R2 culture media (RPMI-1640 completed with 2% of FBS). After the incubation period, non-adherent cells were washed three times with R2 media and adherent monocytes were cultured for 6 days in R10 media (RPMI-1640 completed with 10% FBS) containing GM-CSF and IL-4 (both at 100 ng/mL), renewing half of the media after 3 days. With this protocol, immature DCs (iDCs) were obtained. Non-adherent cells (peripheral blood lymphocytes, PBLs) were washed with PBS and stored in liquid nitrogen until use in allogenic stimulation experiments (see below).

Mature DCs (mDCs) were obtained by incubation of iDCs with bacterial lypopolysacharide (LPS) (10 ng/mL) and interferon-γ (IFN-γ) (100 U/mL) for 48 h. Tolerogenic DCs (tolDCs) were obtained using the same conditions indicated for mDCs but also adding 1α,25-dihidroxyvitamin D3 (50 nM) to the culture media.

2.7. Nanocapsules toxicity on immature DCs

iDCs were incubated for 24 h with the different NCs at increasing final concentrations (25, 50, 100, 200, 400 and 900 μg/mL). After the incubation period, cells were harvested, washed twice with PBS and stained with optimal quantities of vital marker eFluor™660 for 30 min (4 ºC). After washing 3 times with PBS containing bovine serum albumin (BSA) at 2 %, cells were analyzed by flow cytometry in a BD FACSCalibur™ cytometer. Data were analyzed using the Flowing software (Cell Imaging Core, Turku Centre for Biotechnology, Finland). Data were normalized considering the dead cells obtained after iDC incubation in culture media alone.

For Review Only

2.8. Interaction of the nanocapsules with DCs

To evaluate the percentage of the nanosystems that interact with the cells by flow cytometry, $5x10^5$ hDCs were plated into a 24-well plate with 0.5 mL of RPMI 10% FBS. Immediately, DiD-labeled nanosystems were added at a concentration of 100 μg/mL. After 1h of incubation, cells were washed with PBS and fixed in a flow cytometry tube with 200 μL of PBS containing 1% paraformaldehyde (PFA). For acquisition, samples were diluted with 500 μL of PBS and the suspension was analyzed by flow cytometry (Accuri Cytometers, Ann Arbor, MI, USA).

2.9. Human DCs phenotype analysis

To analyze the phenotype of iDCs after incubation with the different NCs, iDCs were incubated with the different nanosystems at a final concentration of 200 μg/mL for either 2 or 24 h. After the activation period, cells were washed twice to eliminate the NCs and incubated up to a total period of 48 h. To determine the iDC phenotype, cells were washed twice with PBS containing BSA (0.1%) and stained with optimal amounts of different antibodies for 30 min, at 4 ºC, in the dark). Levels of maturation markers HLA class II, CD80 and CD83 were quantified by flow cytometry. CD1a was included as a DC marker to verify the correct monocyte differentiation. Cell viability was determined using the vital marker eFluor™660. After washing 3 times with PBS containing BSA at 2%, cells were analyzed by flow cytometry in a BD FACSCalibur™ cytometer. Data were analyzed using the Flowing software (Cell Imaging Core, Turku Centre for Biotechnology, Finland). Data are shown as the ratio between the mean fluorescent intensity (MFI) of the corresponding marker in iDCs incubated with the different NCs and the MFI of iDC incubated in culture media alone.

2.10. Indoleamine 2,3-dioxygenase (IDO) activity in iDCs

IDO activity was determined by quantification of kinurenin in culture media obtained from different DCs (section 2.9) using described methods [24]. Briefly, 4 h before the end of the culture period, L-tryptophan (100 μM) was added to the medium. Culture medium (100 μL) was mixed with 30% trifluoroacetic acid (TFA) (50 μL) to precipitate proteins and cell debris by centrifugation (10.000 g, 5 min, room temperature). Supernatant (75 μL) was mixed with an identical volume of the Ehrlich Reagent and absorbance at 490 nm was determined using a BioRad 680 ELISA reader.

2.11. Lymphocyte activation capacity of iDCs pre-incubated with different NCs

For Review Only

The capacity of iDCs pre-incubated with the different NCs to activate CD8+ T lymphocytes in an allogeneic culture was determined by flow cytometry. Briefly, after incubation of iDCs with the different NCs for 24 h (200 μg/mL), cells were harvested, washed with PBS and plated with allogeneic T cells (non-adherent PBLs obtained after washing adherent monocytes, see above) at a 1:10 ratio (DC:T) for 7-10 days. After the activation and proliferation period, cells were harvested, washed and stained with optimal quantities of CD8 and CD28 antibodies and analyzed by flow cytometry, as indicated above.

2.12. Cytokine secretion by iDCs incubated with different NCs

We used personalized MILLIPLEX®MAP kits containing microparticles to capture IFN-γ, IL-10, IL-12p70, IL-15, IL-1β, IL-2, IL-4, IL-23, IL-27, TNF-α, TNF-β, IL-5 and IL-8 present in culture media, previously stored at -80 ºC. The assay was performed according to the manufacturer instructions (Millipore). Plates were read in a MAGPIX® analyzer (Merk Chemicals & Life Sciences). Cytokines concentration was determined using calibration curves (variable ranges for the different cytokines) and calculated as pg/mL with the exception of IL-4, IL-23, IL-27 and TNF-β calculated as ng/mL. Final data were expressed as the ratio between cytokine secreted by iDCs after treatment with NCs and cytokine secreted by iDCs incubated in media alone (-: ratio ≤ 1; +: ratio 1-2; ++: ratio 2-3; +++: ratio > 3).

2.13. In vivo studies

2.13.1. Animals

$CX_3CR_1^{+/gfp}$ [25] heterozygous mice were obtained from Jackson Laboratories and bred in-house. C57BL/6JRj were obtained from Janvier Laboratories. Mice were housed in the specific pathogen-free animal facility of the Institute for Research in Biomedicine (Bellinzona), in individually ventilated cages and were used between 8 and 12 weeks of age. Animal protocols were approved by the cantonal veterinarian local authorities under the protocol ID: TI28/17, and the experiments were performed in accordance with the Swiss Federal Veterinary Office guidelines and with the EU Directive 2010/63/EU. Quality assessment of the experimental in vivo studies was performed following the Animal Research Reporting In vivo experiments (ARRIVE).

2.13.2. Footpad injection model

For Review Only

Mice were anesthetized with a mixture of ketamine (100 mg/kg bodyweight, Parke Davis) and xylazine (10 mg/kg bodyweight, Bayer). 15 µL of nanosystems were subcutaneously injected 12 hours before sample collection.

2.13.3. Two-Photon Microscopy

For follicular DCs and subcapsular sinus macrophages labeling, $CX_3CR_1^{+/gfp}$ mice were injected in the footpad with 0.5 µg of αCD21/35-Pacific Blue (Biolegend) and αCD169-PE (Biolegend) respectively 2 h before sample collection. PLNs were then collected and mounted on a slide with PBS. Images were acquired with a LaVision Trimscope II upright two-photon microscope (LaVision Biotec) with a 10x (Plan Apo lambda NA 0.45, Nikon) dry objective. Excitation was performed with two Chameleon Vision Ti:Sa lasers (Coherent) tuned at 830 nm and 925 nm respectively. Images were z-stacks or mosaic reconstructions acquired with a pixel size of 1.07 µm and z-step of 3 µm, for a total imaging depth of around 350 µm. Mosaic reconstructions and image analysis were conducted with Fiji-Imagej (ImageJ) and Image Stitching plugin.

2.13.4. Flow Cytometry

A single cell suspension of PLNs from NP-injected C57BL/6JRj was obtained by digestion for 10 minutes at 37°C with an enzyme mix of DNase I (0.28 mg/mL, Amresco), dispase (1 U/mL, Corning), and collagenase P (0.5 mg/ml, Roche) in calcium- and magnesium-free PBS (PBS -/-) followed by a stop solution composed of 2 mM EDTA (Sigma-Aldrich) and 2% heat-inactivated filter-sterilized fetal calf serum (Thermo Fisher Scientific) in PBS -/- (Sigma-Aldrich). Fc receptors were blocked (αCD16/32, BioLegend) followed by surface staining with αMHC II-Pacific Blue, αCD11b-Brilliant Violet 785, αCD11c-Brilliant Violet 711, αF4/80-Alexa 488, αCD169-Brilliant Violet 605 (Biolegend) and analyzed by flow cytometry on an LSRFortessa (BD Biosciences). Cells were gated as follows: CD11b+ DCs, MHC II+ CD11c+ CD11b+; CD11b- DCs, MHC II+ CD11c+ CD11b-; SSM, MHC II+ CD11c intlow CD11b+ CD169+ F4/80-; MM, MHC II+ CD11c intlow CD11b+ CD169+ F4/80+. Data were analyzed using FlowJo software (TriStar).

2.14. Statistical analysis

Unless otherwise indicated, all the experiments were repeated at least 3 times. Results are presented as mean ± standard deviation. The differences were considered significant for * $p < 0.05$, ** $p < 0.01$, *** $p < 0.001$, and **** $p < 0.0001$. All statistical analyses were carried out with Graph- Pad Prism Version 7.0 software.

For Review Only

3. Results

3.1. Development and characterization of inulin-based nanosystems

During the first step in the development of INU NCs, we evaluated different ratios of vitamin E:INU and their impact on the particle size and polydispersity of the resulting nanosystems (**Fig. S1A**). The tested ratios, from 4:1 to 1:1 (vitamin E:INU, w/w), rendered low polydisperse nanometric size particles with an almost neutral zeta potential.

The use of a neutral polysaccharide, such as INU, allowed us to specifically modulate the charge of the nanosystem using ionic co-surfactants. Thus, the use of sodium glycocholate, which is negatively charged, led to INU NCs with a negative charge of approximately – 40 mV (**Fig. S1B** and **S1C**). On the other hand, by using positively charged benzethonium chloride as a co-surfactant, we obtained NCs with a highly positive surface charge of approximately + 40 mV. After this exploratory study, we selected sodium glycocholate as the co-surfactant for further studies, because negatively charged NCs tend to be less toxic than positive ones, and to have better dissemination capacity in the organism [8]. The resulting INU NCs had a particle size of approximately 250 nm and a negative surface charge (**Table 2**, INU NCs M).

Different electron microscopy techniques were used to characterize these new NCs. The Cryo-TEM technique (**Fig. 1A**), which retains the conformation of the nanosystem in the liquid state after its vitrification, revealed round-shape structures with particle sizes between 150 and 300 nm, in agreement with the values obtained by dynamic light scattering (DLS). Using conventional TEM (**Fig. 1B**), it was possible to confirm the globular structure of the NCs.

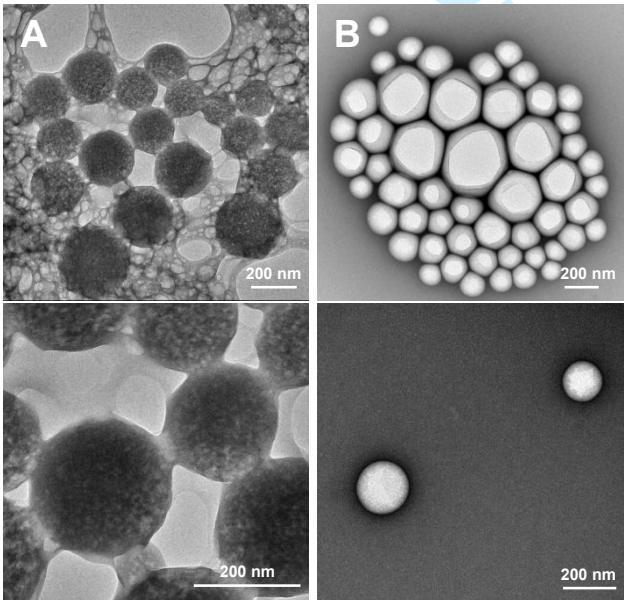

Figure 1. Electron microscopy images of inulin nanocapsules. Different transmission electron microscopy techniques were used to visualize the size and shape of the nanocapsules: Cryo-TEM (A)

and TEM with a negative staining (B).

A second step in the development of lympho-targeted INU NCs involved the reduction of their size below 100 nm. A reduction in the particle size, without a modification of the final concentration of each component, was accomplished by following a modification of the solvent displacement technique, as previously described [26]. Based on our own experience [27,28], CS NCs, with a vitamin E and glycocholate core, were produced also with two different particle sizes (S and M) and adopted as a reference of positively charged NCs (**Fig. 2A**).

Different techniques were used to rigorously characterize the particle size of the four nanosystems, such as the NTA technique (**Fig. 2B**) and DLS (**Table 2**). The results showed that the particle size of NCs S obtained by these techniques was similar (between 70 and 80 nm, approximately). Larger differences were found for INU NCs M, with a particle size of 246 ± 16 nm by DLS and 197 ± 74 nm by NTA.

Table 2. Physicochemical properties of the developed nanosystems. Particle size and PDI were obtained by dynamic light scattering. INU: inulin; CS: chitosan; NCs: nanocapsules; S: small size; M: medium size (n ≥ 10).

Nanosystem	Particle size (nm)	PDI	Z-potential (mV)	pH
INU NCs S	69 ± 6	0.18	- 33 ± 8	6.3 ± 0.2
INU NCs M	246 ± 16	0.12	- 25 ± 11	6.4 ± 0.2
CS NCs S	72 ± 5	0.16	+ 37 ± 4	4.5 ± 0.1
CS NCs M	172 ± 11	0.11	+ 34 ± 4	4.5 ± 0.1

FESEM images, using STEM and InLens detectors, corroborated the differences in the particle size of S and M NCs (**Fig. 2B**).

For Review Only

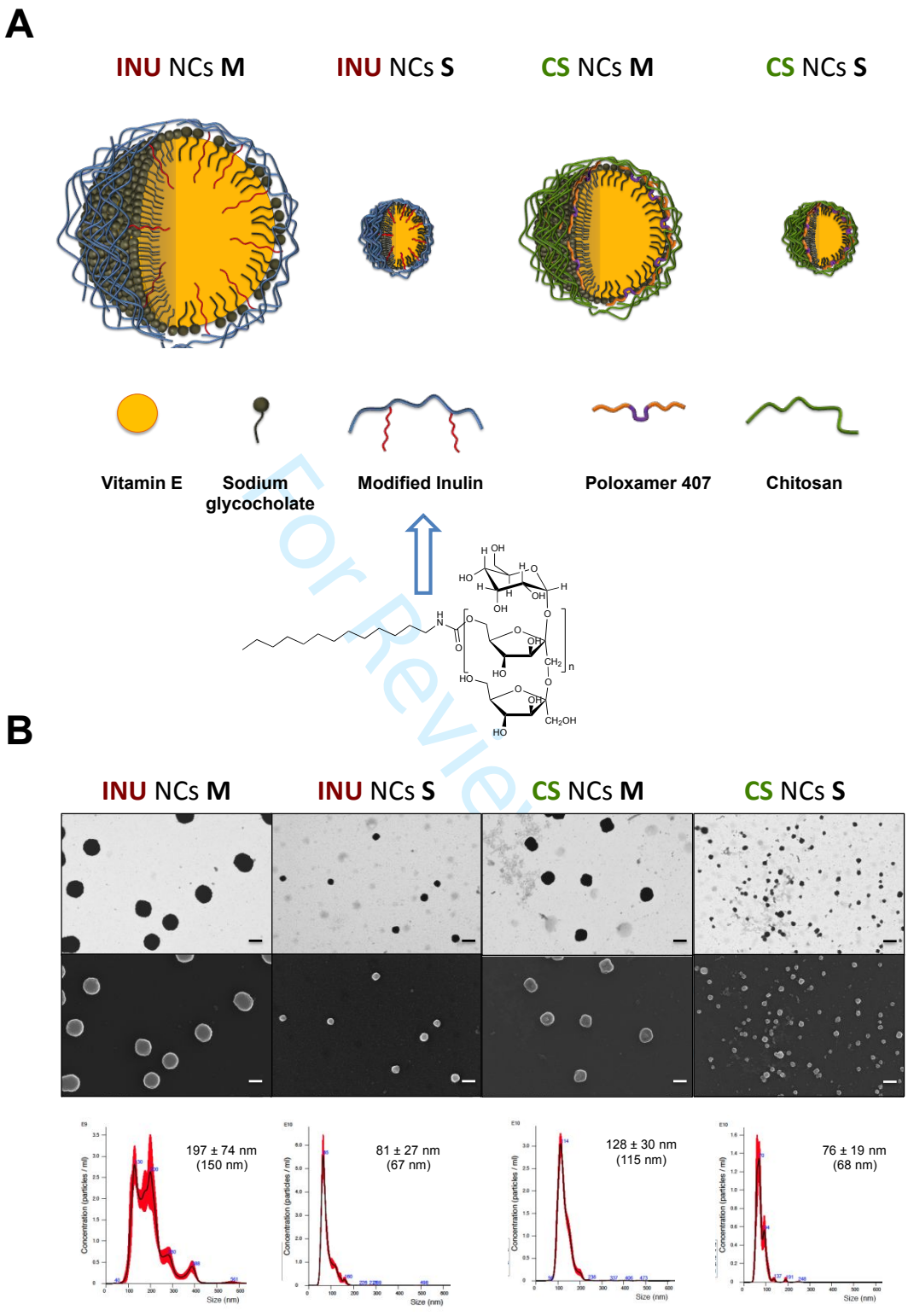

Figure 2. Polymeric nanocapsules (NCs) developed in this work. (A) Illustration of inulin nanocapsules (INU NCs) and chitosan nanocapsules (CS NCs) of two different particle sizes, small (S, ≈ 70 nm) and medium (M, 170 - 250 nm) size. The structure of modified inulin is also showed in the figure. The size scale between the prototypes was maintained in the draw. (B) Field emission scanning electron microscopy (FESEM), using STEM (first row) and InLens (second row) detectors. All scale bars = 200 nm. In the third row, a representative image of the particle size distribution obtained

for each system by nanoparticle tracking analysis (NTA) is shown. The mean particle size with the standard deviation and the mode (between brackets) are indicated in the figure (n=3).

When developing a new nanosystem, apart from obtaining the adequate physicochemical properties, a minimum stability, for operational purposes, has to be guaranteed. For this purpose, the colloidal stability of the nanosystems at 4 ºC was monitored over time. The results showed that the NCs were stable for, at least, 1 month (**Fig. S2**). On the other hand, to guarantee long-term stability, a freeze-drying process was developed. The use of sucrose [27] at a concentration of a 15% allowed the preservation of the particle size after the freeze-drying process (**Fig. S3A**).

3.2. Study of the interaction of NCs with primary human DCs

In this section, we describe the toxicity of the different nanosystems and their capacity to induce activation of human-derived DCs. Before performing these experiments, the stability of the nanosystems in cell culture media was assessed (**Fig. S2B**).

3.2.1. Cytotoxicity

Primary human iDCs were differentiated from monocytes as described in section 2.6. Cells were incubated with different concentrations of either CS or INU NCs for 24 h and stained with a vital label to be analyzed by flow cytometry. As depicted in **Fig. 3**, INU NCs were less toxic compared to CS NCs, being INU NCs M the ones showing the lowest toxicity. Regarding the influence of the size, at the highest tested concentration, S NCs showed a tendency to be more toxic than M NCs.

For Review Only

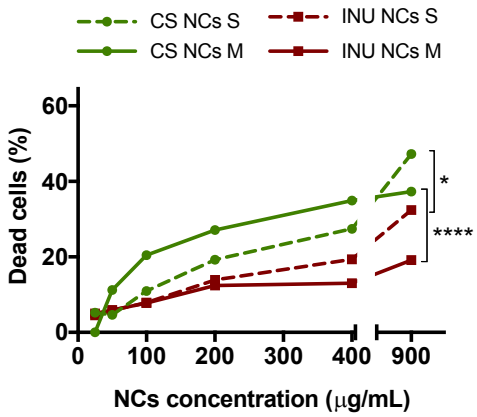

Figure 3. Chitosan (CS) and inulin (INU) nanocapsules (NCs) cytotoxicity on immature dendritic cells (iDCs). iDCs were incubated with either CS (green lines) or INU (red lines) NCs at different concentrations during 24 h. Small (S, ≈ 70 nm) (dashed lines) and medium (M, 170 - 250 nm)(continuous lines) size NCs were tested. After the incubation period, cells were harvested, washed and stained with a vital label. Results were normalized with the percentage of dead iDCs incubated in culture media alone. Each point represents the mean of four different donors. For the statistical analysis the area under the curve for each nanosystem was calculated and the differences between the particles size (S *vs* M) and the polymer shell (CS *vs* INU) analyzed using a One-way ANOVA followed by a Tukey test. Significance levels * $p < 0.05$ and **** $p < 0.0001$.

3.2.2. Interaction cell-nanosystems

After establishing a non-toxic dose, NCs were labeled with DiD to evaluate their interaction with iDCs, at 100 μg/mL. The incorporation of the fluorophore did not alter the particle size of the NCs (**Fig. S4**). The analysis by flow cytometry (**Fig. 4A-C**) showed a size-dependent effect, in particular for INU NCs, where S particles (70 nm) were found to interact with iDCs in a higher extent than the M size ones (250 nm) (**Fig. 4A and C**). However, no significant differences were observed between CS NCs S (70 nm) and CS NCs M (170 nm) and their interaction with iDCs was similar to the one of INU NCs S. On the other hand, with regard to the influence of the polymer shell, we observed a higher interaction for positive NCs for the M sizes, but not for the S ones. In terms of mean fluorescence per cell, INU NCs S showed the highest mean fluorescence intensity value (MFI) (**Fig. 4B**).

For Review Only

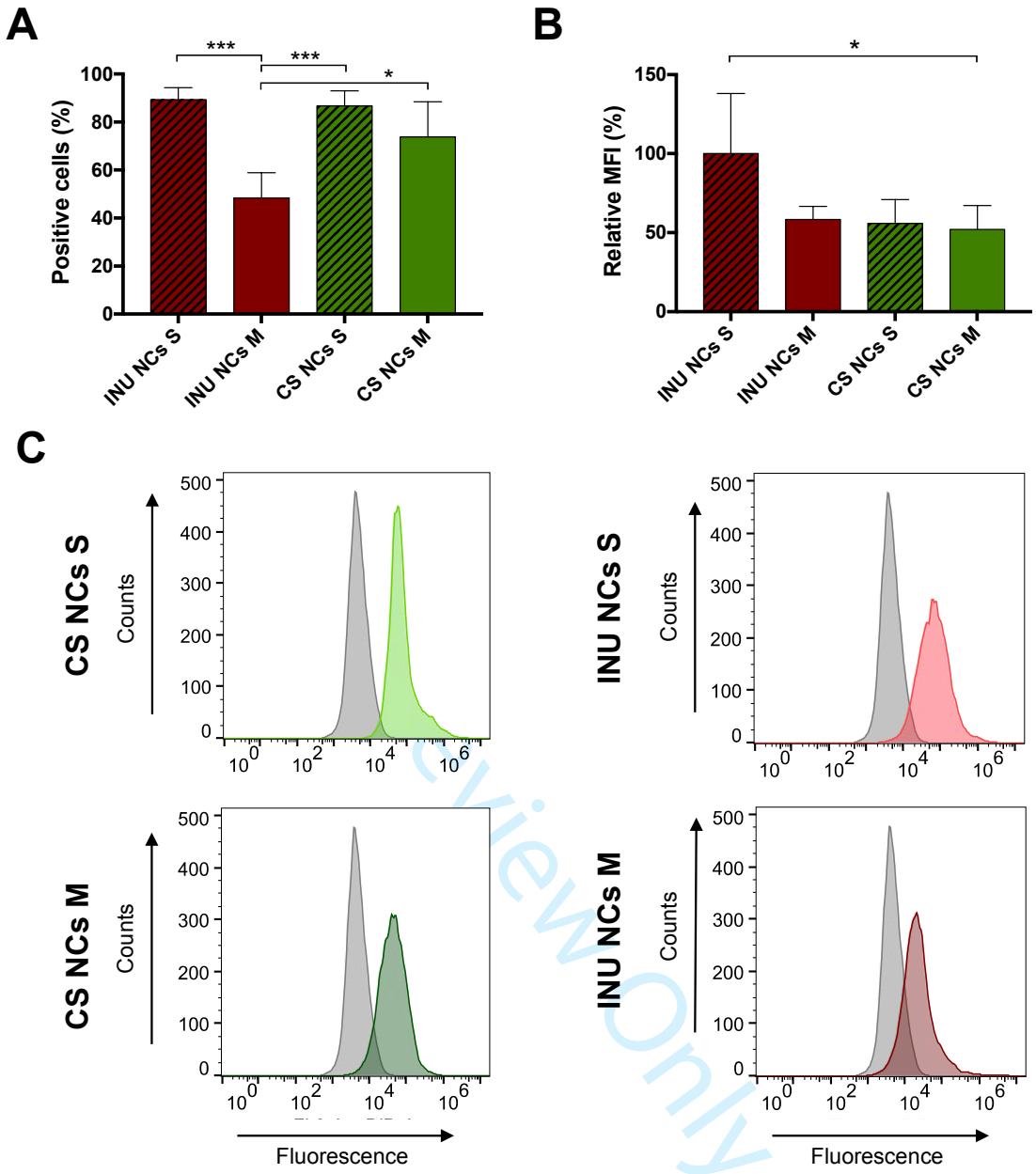

Figure 4. Interaction of the different labeled nanosystems with iDCs. After incubation of iDCs with the different NCs, the percentage of positive cells (A) and mean fluorescence intensity (B) were analyzed. Representative flow cytometry histograms showing the interaction of the four nanosystems at 100 µg/mL after 1 h incubation with iDCs is shown in C. In grey non-treated cells are represented. Inulin-based nanocapsules (INU NCs) and chitosan nanocapsules (CS NCs) of two different sizes, small (S, ≈ 70 nm) and medium (M, 170 – 250 nm) were tested. Statistical analysis was done using a one-way ANOVA followed by a Tukey test. Significance levels * $p < 0.05$ and *** $p < 0.001$.

3.2.3. Change in iDCs phenotype

To evaluate the effect that NCs have on iDC phenotype, different cell markers were analyzed by flow cytometry after incubation with the four NCs at 200 µg/mL. After 2 h incubation, both, S and M, CS NCs (**Fig. 5A**) showed a higher capacity of DC activation compared to INU NCs (**Fig. 5B**) causing a greater increase in the expression of CD80 and CD83 maturation markers. After 24 h, DCs incubated with CS NCs still showed a tendency of up-regulation of CD80 and CD83 activation markers but without reaching statistical significance (**Fig. 5C**). In the case of INU NCs, only the small particles showed a significant slight increase in the upregulation of CD83 (**Fig. 5D**). Regarding the particle size, similar values were found for S and M NCs.

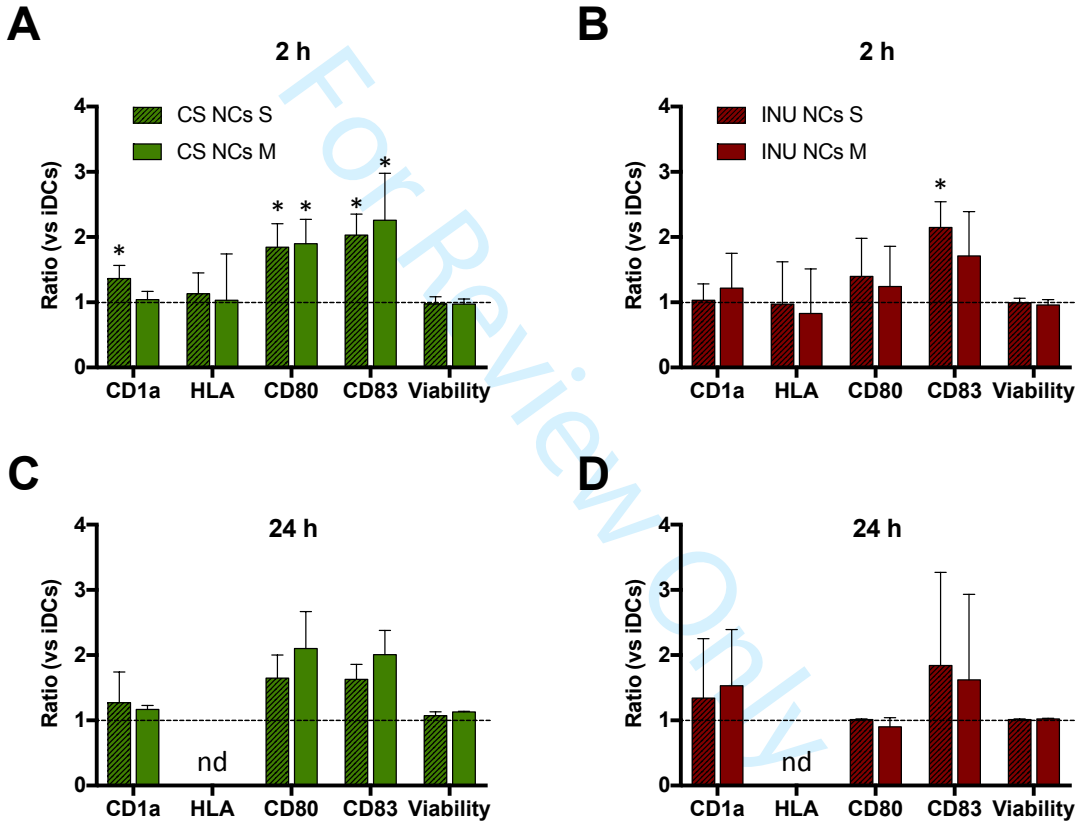

Figure 5. Dendritic cell (DC) phenotype induced by incubation with chitosan (CS) and inulin (INU) nanocapsules (NCs). Immature DCs (iDCs) were incubated with either CS (A, C) or INU (B, D) NCs at 200 µg/mL. Incubation was performed for 2 or 24 h. Small (S, ≈ 70 nm) and medium (M, 170 – 250 nm) size NCs were tested. After the incubation period, cells were stained with different antibodies and analyzed by flow cytometry. Results are shown as the ratio between the iDCs incubated with NCs *vs* iDCs incubated in culture media. *: ratio significantly higher than 1 ($p<0.05$; Student´s T Test). No significant differences were found between the capacity of the four NCs to modify the expression of the different markers (one-way ANOVA). n.d. Not determined.

For Review Only

The fact that INU NCs hardly showed a capacity of DCs activation *in vitro*, led us to speculate about their potential to induce a tolerogenic phenotype on iDCs. To evaluate this hypothesis we quantified the 2,3-Indoleamine dioxigenase (IDO) enzymatic activity (**Fig. 6A**). IDO activity in iDCs treated with the four different NCs was similar to that observed in both immature and mature DCs (**Fig. 6A**, iDCs and mDCs respectively) and significantly lower to that observed in DCs incubated with vitamin D3 (**Fig. 6A,** tolDCs), an agent known to induce IDO expression.

3.2.4. Stimulation of CD8+ T lymphocytes

Next, we evaluated the capacity of iDCs pre-incubated with the NCs, at 200 μg/mL, to activate allogeneic CD8+ T lymphocytes *in vitro* (**Fig. 6B**). The results showed that pre-incubation of iDCs with the NCs significantly increased the percentage of activated CD8+ T lymphocytes (determined as CD28+ cells). Both, size and composition were found to influence this response. CS NCs S showed the highest level of CD8+ T lymphocyte responses.

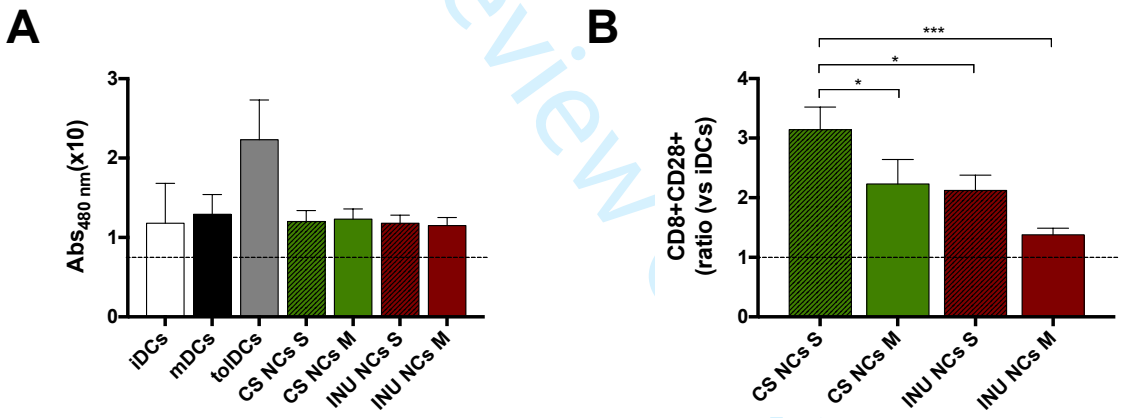

Figure 6. 2,3-Indoleamine dioxigenase (IDO) activity and T cell activation capacity by immature dendritic cells (iDCs) incubated with different nanocapsules (NCs). (A) iDCs from four different donors were incubated with either chitosan (CS) or inulin (INU) NCs at 100 μg/mL for 2 h. Small (S, ≈ 70 nm) and medium (M, 170 – 250 nm) size NCs were tested. The IDO enzymatic activity was determined by the quantification of kinurenin in culture media [24]. Data are shown as the absorbance at 490 nm. Addition of vitamin D3 to iDCs was used to induce a tolerogenic phenotype (tolDCs). iDCs and mature DCs (mDCs) were used as controls. (B) The capacity of the treated iDCs to activate allogeneic CD8+ T lymphocytes was determined by flow cytometry quantifying the up-regulation of CD28. Results are shown as the ratio between the percentage of CD8+CD28+ T cells using iDCs incubated with NC *vs* percentage of CD8+CD28+ T cells using iDCs incubated in culture media. With the only exception of INU NCs M (p=1.0, one-way ANOVA, Bonferroni post hoc) all the NCs significantly increased the percentage of activated CD8+ T lymphocytes compared to non-treated iDCs (NCs CS S, p=0.0001; NCs CS M, p=0.006; NCs INU S,

p=0.012; one-way ANOVA, Bonferroni post hoc)(data not shown in the graph). From the four NCs evaluated, CS NCs S showed the higher capacity of CD8 T lymphocyte stimulation (one-way ANOVA, Bonferroni post hoc). The differences were considered significant for * $p < 0.05$, ** $p < 0.01$, *** $p < 0.001$ and **** $p < 0.0001$.

3.2.5. Cytokine secretion

To deeper analyze the kind of activation that the different nanosystems induce on iDCs, we quantified the amount of cytokines secreted to the culture media by iDCs incubated with the different NCs for 24 h. A summary of the results, in **Table 3**, indicates that CS NCs induced a higher cytokine secretion (ratios >1) by iDCs compared to INU NCs, with the exceptions of IL-8 where similar secretion for both types of prototypes was observed. No effect of the particle size in the secretion of the cytokines was noted.

Table 3. Cytokine secretion by iDCs after incubation with different nanocapsules (NCs).

Cytokine*	CS NCs S	CS NCs M	INU NCs S	INU NCs M
IFN-γ	+	+	-	-
IL-10	+	++	-	-
IL-12p70	-	-	-	-
IL-5	+++	+++	-	-
IL-8	+	+	+	+
TNF-α	-	-	-	-
TNF-β	+++	+++	+	+

* Data are expressed as the ratio between cytokine secreted by iDCs after treatment with NCs and cytokine secreted by iDCs incubated in media alone. Symbols: -: ratio ≤ 1; +: ratio 1-2; ++: ratio 2-3; +++: ratio > 3.

3.3. Lymphatic drainage of inulin and chitosan NCs in mice

DiD-labeled NCs were injected into the footpad of mice and the accumulation of the nanostructures in the PLN (**Fig. 7A** and **7B**) was evaluated using two different techniques, flow cytometry (**Fig. 7C**) and 2PM (**Fig. 7D**).

The results in **Fig. 7** indicate that at 12 h post-injection the four nanosystems were capable of reaching the PLN, independently of their size and charge. However, using both, flow cytometry and the 2PM studies, we observed that INU NCs S reached the PLN in a significantly higher extent than the rest of the prototypes.

On the other hand, with regard to the biodistribution inside the LN, the accumulation of the NCs mainly occurred in the medullar region (**Fig. 7**). The images of the excised PLNs also

For Review Only

showed this distribution (**Fig. 7E**): DiD-labeled NCs are shown in white and the follicles can be discerned by the presence of subcapsular sinus macrophages (SSM) (red cells) covering these areas. In the green channel, cells of myeloid origin expressing CX3CR1 were visualized.

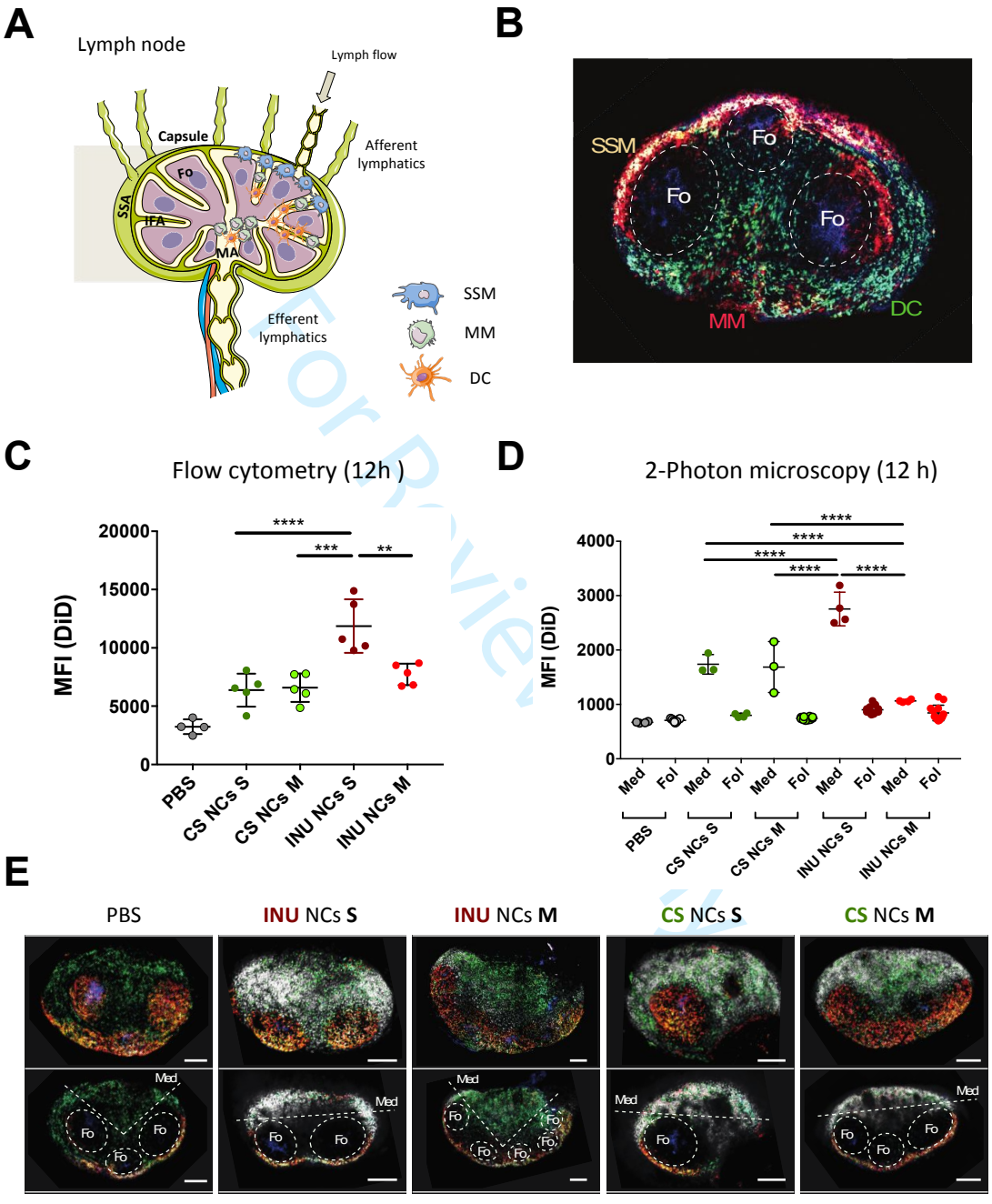

Figure 7. Accumulation of the different nanosystems in the popliteal lymph nodes (PLNs). (A) Schematic drawing representing the anatomical position of the major phagocytic populations in the LN. Subcapsular sinus macrophages (SSM) are located in the sub capsular sinus area (SSA) in close proximity to the B cell follicles (Fo), while Medullary Macrophages (MM) are mainly located in the medullary area (MA) as well as the interfollicular region (IFA). This schematic drawing has been modified from the original work provided by Servier Medical Art (https://smart.servier.com/). (B) 2-photon micrograph

showing the phagocytic populations of the lymph node based of the expression of the markers CD169 (red) and CX3R1 (green), SSM (CD169+, CX3CR1+), DC(CD169-, CX3CR1+), MM(CD169+, CX3CR1-). (C) Chitosan (CS) and inulin (INU) DiD-labeled NCs of two different sizes (S, ≈ 70 nm and M, 170 – 250 nm) were injected in the footpad of $CX_3CR_1^{+/gfp}$ and C57BL/6JRj mice (5 animals per group). After 12 hours, the PLNs from C57BL/6JRj were digested and the mean fluorescence intensity (MFI) evaluated by flow cytometry. (D) PLNs from $CX_3CR_1^{+/gfp}$ mice were evaluated using 2-photon microscopy (2PM). With this technique the MFI of each nanosytem in the medullar (Med) and the follicular (Fol) region was quantified. In E, a representative image of the PLNs. Upper row shows a maximum intensity projection of the whole z-stack of the lymph node, while lower row shows a slice with the different regions highlighted. SSM (CD169+) are shown in red, nanocapsules (NCs) in white, in blue the follicular DCs (CD21/35+) and in green cells of myeloid origin expressing CX_3CR_1 receptor. One-way ANOVA, Brown-Forsythe test. To simplify the interpretation, the comparisons were made only between the groups injected with NCs. The differences were considered significant for * $p < 0.05$, ** $p < 0.01$, *** $p < 0.001$ and **** $p < 0.0001$.

3.3.1. NCs capture by different subsets of immune cells

The results of the percentage of positive cells and mean fluorescence intensity (MFI) associated to the uptake of the DiD-loaded NCs by the different cell populations are shown in **Fig. 8A-D**. It can be noted that the majority of SSM, MM and CD11b+ DCs were positive for DiD, this meaning that they captured and/or interacted with the NCs, whereas lower percentages were detected in CD11b- DCs. However, MM showed a higher MFI than SSM, also observed in the reconstruction of the PLNs (**Fig. 7E**). Regarding DCs, CD11b+ DCs interacted with more NCs than CD11b-.

Among the different NCs, INU NCs S were the ones captured to a higher extent by all the cell subtypes confirming the results showed in **Fig. 7**. On the other hand, CS NCs S showed higher counts (similar to INU NCs S) of positive CD11b+ DCs although the MFI was still higher for INU NCs S (**Fig. 8C**).

For Review Only

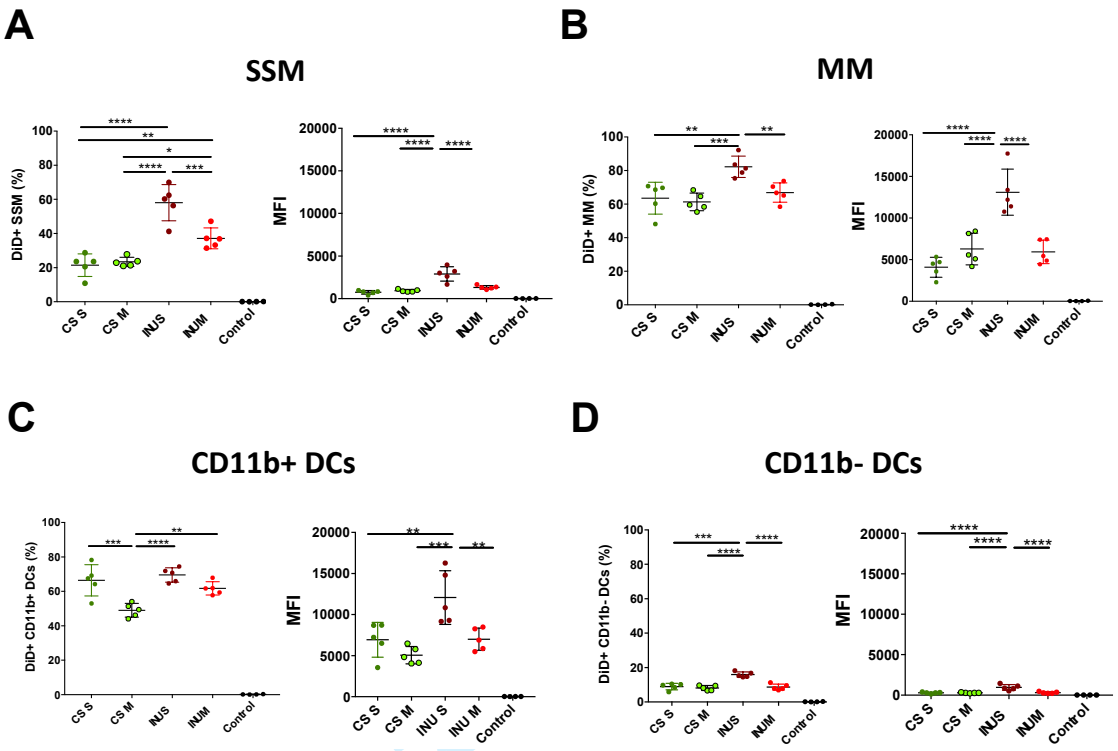

Figure 8. Interaction of the nanocapsules (NCs) the different subsets of immune cells in the popliteal lymph node (PLN). Chitosan (CS) and inulin (INU) NCs of two different sizes (S, ≈ 70 nm and M, 170 – 250 nm) were injected in the footpad of B6 mice (5 animals per group). After 12 hours the PLNs were collected, enzymatically digested and stained with an antibody panel specific to, macrophages (MHC II+, CD11b+, CD11c intlow, CD169+, and F4/80 positive in medullary macrophages, MM, and negative in subcapsular sinus macrophages, SSM) and dendritic cells (DC, MHC II+, CD11c+, CD11b positive or negative population). Percentage of DiD+ cells and the mean fluorescence intensity (MFI) are represented for each subset of immune cells. Analysis: all statistical analyses were performed assessing normal distribution of samples (Saphiro-Wilk test) and applying a one-way ANOVA test. * $p < 0.05$, ** $p < 0.01$, *** $p < 0.001$, **** $p < 0.0001$.

For Review Only

4. Discussion

INU microparticles have reached phase 2 in clinical trials as an adjuvant for vaccination [3–5]. Yet, despite this achievement and the extensive use of INU in pharmaceutical industry, this neutral polysaccharide has barely been explored as antigen delivery nanocarrier [22]. The objective of this work was to build a new delivery vehicle based on a non-ionic INU-based polymeric surfactant and to explore its use for the targeting towards specific phagocytic populations in the lymphatic system. The delivery carrier was selected based on the knowledge generated by our group on polymeric NCs consisting of an oily core and a polymeric shell [27,29,30]. As an oil for the NC's core, we selected vitamin E, based on its reported

immunoregulatory properties [31]. In a first step, a screening of different ratios of vitamin E:INU led to the formation of NCs with a neutral zeta potential and a particle size of 250 nm. The inclusion of an anionic co-surfactant allowed the preparation of negatively charged INU NCs. A second step in the development of lympho-targeted INU NCs involved the reduction of their size below 100 nm, using a technology developed by our own group [26]. The rationale behind this step is that 100 nm is considered the threshold for an adequate access of nanoparticulated materials through the interstitial channels to the lymphatics [15,32,33]. In that way, two different particle sizes INU NCs were developed: S, 70 nm and M, 250 nm. Taking into consideration that CS NCs have been widely explored to enhance the immunogenicity of specific antigens [27,34,35], for comparative purposes, we developed CS NCs, with a similar core composition and particle sizes than those of INU NCs.

The characterization of the panel of NCs was performed using complementary techniques. The NTA, which correlates the Brownian motion of individual particles recorded with a camera with their particle size, supplemented the measurements done by DLS, where an average of the fluctuations in the scattered light is related with that size. The results showed that the particle size of NCs S obtained by these techniques was similar (between 70 and 80 nm, approximately). However, the particle size of NCs M was 246 ± 16 nm by DLS and 197 ± 74 nm by NTA, for INU NCs. This difference could be related to the size polydispersion observed by the last technique. Besides, the different electron microscopy techniques confirmed the differences between the S and M NCs. The round-shape structure of CS and INU NCs was similar, independently of the nature of the polysaccharide shell (**Fig. 2B**).

One of the critical aspects when developing antigen nanocarriers is their interaction with the immune cells. DCs are the main antigen presenting cells (APCs) in our immune system. After antigen capture, DCs mature and go to LNs where they process and present the antigen to T cells generating an immune response [36]. Thus, the understanding of the interaction of the NCs with DCs is important in order to assess their potential as antigen carriers. The results of toxicity in primary human DCs showed a lower toxicity for INU NCs than for CS NCs. Regarding the particle size, at least for high concentrations, the M NCs showed a tendency to be less toxic than S NCs. These results correlated with the fact that the S NCs interacted in a higher degree with the DCs (**Fig. 4A**), and are in agreement with the majority of the research regarding NPs uptake by DCs, showing a preference for small particle sizes [37–39]. On the other hand, with regard to the influence of the polymer shell of the NCs in their interaction with DCs, based on the literature, we could presume that positive particles would interact in a higher degree compared to the negative ones [38,40]. This was the case for NCs M, but not for the S ones. Surprisingly, in terms of mean fluorescence per cell, INU NCs S

For Review Only

showed the highest mean fluorescence intensity value (MFI) (**Fig. 4B**). Despite the low level of significance of this difference, the higher interaction of INU NCs S as compared to CS NCs S highlights the fact that the surface charge is not the only factor -in addition to the size- influencing the interaction, and that the composition may ultimately drive particle-cell interaction.

CS NCs (**Fig. 5A**) showed a higher capacity of DC activation compared to INU NCs (**Fig. 5B**) causing a greater increase in the expression of CD80 and CD83 maturation markers. These results agree with previous studies that have shown the activation of these two markers in DCs by different CS NPs [41,42]. In the case of INU NCs, only the small particles showed a slight increase in the upregulation of CD83 (**Fig. 5D**). The activation of DCs by INU NCs has hardly been reported. Only one study has disclosed the capacity of OVA-loaded INU acetate NPs to upregulate CD80 [22]. The higher upregulation of activation markers caused by CS NCs as compared to INU NCs could be partially related to their higher toxicity, as shown in **Fig. 3**. Despite the limited activation that we found, none of the evaluated NCs induced a tolerogenic DC phenotype as shown in the IDO enzymatic activity assay (**Fig. 6A**). IDO activity has been linked to suppression of both innate and adaptive immunity promoting immune tolerance through the catabolism of tryptophan and other indole compounds [43].

CD8+ T cells are pivotal elements for the defense of intracellular pathogens and for tumor surveillance and they are considered critical targets in the development of vaccines against cancer and chronic infectious diseases, such as HIV [44,45]. In this study, CS NCs S showed the highest level of CD8+ T lymphocyte responses (**Fig. 6**). This is in agreement with the theory that indicates that small NPs, due to their resemblance with the size of a virus, are processed like them, following similar endocytic routes, leading to a strong CD8+ T-cell responses [46]. Indeed, this was previously observed for OVA-conjugated polystyrene NPs [47] and OVA-loaded silica NPs [48].

To deeper analyze the kind of activation that the different nanosystems induce on iDCs, we quantified the amount of cytokines secreted to the culture media by iDCs incubated with the different NCs for 24 h. The results, in **Table 3**, indicate that, in general, CS NCs induced a higher cytokine secretion (ratios >1) by iDCs. The induction of cytokines secretion by CS formulations has been previously reported [49,50], although in the case of highly purified CS the level of cytokines has generally been low [42]. Similarly, the capacity of INU to promote cytokines secretion has been reported to be low [51].

In summary, the *in vitro* data suggest a clear difference between the CS and INU NCs in terms of DCs activation. Compared with INU NCs, CS NCs caused a higher up-regulation of different activation markers, stimulated the secretion of higher levels of cytokines and

For Review Only

demonstrate a higher capacity of CD8+ T cell activation. The mechanism of action is supposed to be related with the activation of the cGAS-STING pathway and the NLRP3 inflammasome by CS [52]. These data reinforce the idea that CS NCs triggered a more prominent immune activation *in vitro* compared to INU NCs, although this activation could be partially attributed to their higher toxicity. However, this does not necessarily mean that INU NCs cannot have and adjuvant effect *in vivo*. In contrast with other compounds, INU microparticles, with proven adjuvant capacity, have not shown the capacity to activate innate immune receptors such as Dectin-1, TLRs or the inflammasome. Instead, they were recently found to modulate directly the DCs function, resulting in an improved antigen presentation to T and B cells *in vivo* through a non-inflammatory mechanism [53–55], despite the lack of DCs activation *in vitro* [54], and this could be also the case for INU NCs. In fact, these data corroborate the previous statement that adjuvant carriers with the capacity to reach the lymphatic system do not need to induce an inflammation to attract peripheral DCs to the injection site, avoiding in that way an important cause of toxicity [56].

As discussed above, recent data support the hypothesis that free drainage of nanosystems to the LNs can improve the efficacy of vaccines [8]. These nanostructures, usually with particles sizes less than 100 nm, have shown to favor cross-presentation when interacting with the resident DCs in the LNs, triggering an important cellular response [14,15]. Besides, the direct interaction with B-cells can also improve the humoral branch of the immune response [57]. Based on this information and previous studies showing the faster lymphatic drainage of small CS NCs (90 nm) as compared to the medium size ones (240 nm) [58], we performed a systematic study of the influence of the particle size and the polymeric shell of the NCs on their drainage towards the LNs and accumulation in different subsets of resident immune cells using 2PM. This is an emerging technique in the nanotechnology field that enables a high-resolution visualization of the interactions of nanomaterials with cells [59,60]. Apart of 2PM, the results were validated by flow cytometry. With both techniques, we observed that INU NCs S reached the PLN in a higher extent than the rest of the prototypes. The small size of INU NCs S (70 nm) might explain the difference in their drainage with respect to INU NCs M (250 nm). On the other hand, the higher lymphatic drainage with respect to that of CS NC, regardless of the size, could be related to the positive charge of the latest ones, which might favor the retention at the injection site. Overall, we could conclude that both, small size together with negative charge where determinant factors of the improved lymphatic drainage of S INU NCs. Our data agree with those previously reported by other authors showing the capacity of model and biodegradable particles below 100 nm to freely drain to LNs [20,61,62].

For Review Only

On the other hand, with regard to the biodistribution inside the LN, the accumulation of the NCs mainly occurred in the medullar region (**Fig. 7**). This was probably associated with the presence of different population of highly phagocytic cells such as medullary macrophages (MM) and different subtypes of LN resident DCs [63]. The images of the excised PLNs also showed this distribution (**Fig. 7E**): DiD-labeled NCs are shown in white and the follicles can be discerned by the presence of subcapsular sinus macrophages (SSM) (red cells) covering these areas. In the green channel, cells of myeloid origin expressing CX3CR1 were visualized. These results are in accordance with previous experiments performed by us [58] and other groups [20], showing the accumulation of the nanosystems in the medulla of the LN. The time point selected for the analysis, 12 h, appropriate to evaluate the initial accumulation of the NCs in the PLNs, explains the absence of NCs in the B follicles. At this early time, the machinery of the adaptive immune system has not started to operate yet. The dynamics of the NCs – immune cells interaction at larger time points and the implications on the generated immune response will be the subject of future studies.

The immune response induced by NPs upon their interactions with different cell subsets maybe different, not only in intensity but also on the type of immune response (cellular vs humoral, activation vs tolerogenic, etc.) [64,65]. The results of the percentage of positive cells and mean fluorescence intensity (MFI) associated to the uptake of the DiD-loaded NCs by the different cell populations are shown in **Fig. 8A-D**. It can be noted that the majority of SSM, MM and CD11b+ DCs were positive for DiD, this meaning that they captured and/or interacted with the NCs, whereas lower percentages were detected in CD11b- DCs. However, MM showed a higher MFI than SSM, also observed in the reconstruction of the PLNs (**Fig. 7E**), something expected due to the higher avidity of MM to capture lymph-borne particulates when compared with SSM, that are less phagocytic [63,66]. SSM are strategically positioned at the entrance of the LN and they are the first cells encountering and phagocytizing material carried by the afferent lymphatics. Due to their location, SSM can present antigens straight to the B-cells in the underlying follicles [67,68]. The NCs interaction with this type of macrophages might initiate the primary antibody response when using antigen-loaded NCs.

Regarding DCs, CD11b+ DCs interacted with more NCs than CD11b-, probably due to their activation state caused by resident macrophages [69]. A specialized population of CD11b+ have been shown to present associated antigens to T lymphocytes, inducing T cell responses much sooner than and independently of migratory DCs [70]. These results support our hypothesis that the lymphatic targeting of antigen-loaded nanocarriers could contribute to

For Review Only

a more effective host defense. Besides, CD11b+ DCs not only appear to be particularly efficient in the activation of antigen-specific CD4 T cells but can also interact with CD8 T cells [71].

Among the different NCs, INU NCs S were the ones captured to a higher extent by all the cell subtypes confirming the results showed in **Fig. 7**. On the other hand, CS NCs S showed higher counts (similar to INU NCs S) of positive CD11b+ DCs although the MFI was still higher for INU NCs S (**Fig. 8C**). Similarly to these findings, Gerner et al. found that CD11b+ preferentially captured positively charged 40 nm beads [70]. On the other hand, the influence of the particle size in this subset of cells is similar to our in vitro findings, with small particles having a higher interaction than medium size ones. Probably, in these cells, a combined influence of the particle size and the surface charge in the uptake is more emphasized than in the others.

5. Conclusions

Achieving an effective lymphatic accumulation of NPs could be of capital importance for designing modern vaccines. It is well known that the particle size of the nanosystems influences their uptake by the immune cells and the lymphatic drainage. However, the concomitant influence of the particle size and other factors, such as the surface charge inherent to the particle composition, makes it very difficult to withdraw general assertions. An overall conclusion from this work is that, irrespective of their composition (CS NCs vs. INU NCs), small NCs favored both, cell uptake and biodistribution. INU NCs showed less toxicity than their CS counterparts, despite, in the case of small sizes, presenting a higher interaction with dendritic cells. The lymphatic drainage after subcutaneous administration showed that small INU NCs accumulated in a higher extent in the LNs as compared with the rest of the prototypes. This, together with the recent evidence that INU may operate by a non-inflammatory mechanism, explaining its low reactogenicity, convert INU NCs S in an interesting prototype to develop new nanovaccines with lympho-targeting properties.

Summary points

- Modified inulin is a biomaterial that allows engineering polymeric nanocapsules.
- Inulin nanocapsules can be prepared with a tunable surface charge and particle size, in the 70 – 250 nm range.

For Review Only

- Small nanocapsule size facilitates interaction with phagocytes.
- Inulin nanocapsules are less toxic than chitosan nanocapsules to dendritic cells.
- Chitosan nanocapsules cause a higher activation of dendritic cells than inulin nanocapsules.
- All the tested nanocapsules accumulate in the popliteal lymph nodes but to a different extent.
- Inulin nanocapsules of 70 nm shows the highest accumulation in the lymph nodes.
- Nanocapsules show preferential accumulation by different subsets of immune cells.

- **Figure legends**

Figure 1. Electron microscopy images of inulin nanocapsules. Different transmission electron microscopy techniques were used to visualize the size and shape of the nanocapsules: Cryo-TEM (A) and TEM with a negative staining (B).

Figure 2. Polymeric nanocapsules (NCs) developed in this work. (A) Illustration of inulin nanocapsules (INU NCs) and chitosan nanocapsules (CS NCs) of two different particle sizes, small (S, ≈ 70 nm) and medium (M, 170 - 250 nm) size. The structure of modified inulin is also showed in the figure. The size scale between the prototypes was maintained in the draw. (B) Field emission scanning electron microscopy (FESEM), using STEM (first row) and InLens (second row) detectors. All scale bars = 200 nm. In the third row, a representative image of the particle size distribution obtained for each system by nanoparticle tracking analysis (NTA) is shown. The mean particle size with the standard deviation and the mode (between brackets) are indicated in the figure (n=3).

Figure 3. Chitosan (CS) and inulin (INU) nanocapsules (NCs) cytotoxicity on immature dendritic cells (iDCs). iDCs were incubated with either CS (green lines) or INU (red lines) NCs at different concentrations during 24 h. Small (S, ≈ 70 nm) (dashed lines) and medium (M, 170 - 250 nm)(continuous lines) size NCs were tested. After the incubation period, cells were harvested, washed and stained with a vital label. Results were normalized with the percentage of dead iDCs incubated in culture media alone. Each point represents the mean of four different donors. For the statistical analysis the area under the curve for each nanosystem was calculated and the differences between the particles size (S *vs* M) and the polymer shell (CS *vs* INU) analyzed using a One-way ANOVA followed by a Tukey test. Significance levels * $p < 0.05$ and **** $p < 0.0001$.

Figure 4. Interaction of the different labeled nanosystems with iDCs. After incubation of iDCs with the different NCs, the percentage of positive cells (A) and mean fluorescence intensity (B) were analyzed. Representative flow cytometry histograms showing the interaction of the four nanosystems at 100

For Review Only

µg/mL after 1 h incubation with iDCs is shown in C. In grey non-treated cells are represented. Inulin-based nanocapsules (INU NCs) and chitosan nanocapsules (CS NCs) of two different sizes, small (S, ≈ 70 nm) and medium (M, 170 – 250 nm) were tested. Statistical analysis was done using a one-way ANOVA followed by a Tukey test. Significance levels * $p < 0.05$ and *** $p < 0.001$.

Figure 5. Dendritic cell (DC) phenotype induced by incubation with chitosan (CS) and inulin (INU) nanocapsules (NCs). Immature DCs (iDCs) were incubated with either CS (A, C) or INU (B, D) NCs at 200 µg/mL. Incubation was performed for 2 or 24 h. Small (S, ≈ 70 nm) and medium (M, 170 – 250 nm) size NCs were tested. After the incubation period, cells were stained with different antibodies and analyzed by flow cytometry. Results are shown as the ratio between the iDCs incubated with NCs *vs* iDCs incubated in culture media. *: ratio significantly higher than 1 ($p<0.05$; Student´s T Test). No significant differences were found between the capacity of the four NCs to modify the expression of the different markers (one-way ANOVA). n.d. Not determined.

Figure 6. 2,3-Indoleamine dioxigenase (IDO) activity and T cell activation capacity by immature dendritic cells (iDCs) incubated with different nanocapsules (NCs). (A) iDCs from four different donors were incubated with either chitosan (CS) or inulin (INU) NCs at 100 µg/mL for 2 h. Small (S, ≈ 70 nm) and medium (M, 170 – 250 nm) size NCs were tested. The IDO enzymatic activity was determined by the quantification of kinurenin in culture media [24]. Data are shown as the absorbance at 490 nm. Addition of vitamin D3 to iDCs was used to induce a tolerogenic phenotype (tolDCs). iDCs and mature DCs (mDCs) were used as controls. (B) The capacity of the treated iDCs to activate allogeneic CD8+ T lymphocytes was determined by flow cytometry quantifying the up-regulation of CD28. Results are shown as the ratio between the percentage of CD8+CD28+ T cells using iDCs incubated with NC *vs* percentage of CD8+CD28+ T cells using iDCs incubated in culture media. With the only exception of INU NCs M ($p=1.0$, one-way ANOVA, Bonferroni post hoc) all the NCs significantly increased the percentage of activated CD8+ T lymphocytes compared to non-treated iDCs (NCs CS S, $p=0.0001$; NCs CS M, $p=0.006$; NCs INU S, $p=0.012$; one-way ANOVA, Bonferroni post hoc)(data not shown in the graph). From the four NCs evaluated, CS NCs S showed the higher capacity of CD8 T lymphocyte stimulation (one-way ANOVA, Bonferroni post hoc). The differences were considered significant for * $p < 0.05$, ** $p < 0.01$, *** $p < 0.001$ and **** $p < 0.0001$.

Figure 7. Accumulation of the different nanosystems in the popliteal lymph nodes (PLNs). (A) Schematic drawing representing the anatomical position of the major phagocytic populations in the LN. Subcapsular sinus macrophages (SSM) are located in the sub capsular sinus area (SSA) in close proximity to the B cell follicles (Fo), while Medullary Macrophages (MM) are mainly located in the medullary area (MA) as well as the interfollicular region (IFA). This schematic drawing has been modified from the original work provided by Servier Medical Art (https://smart.servier.com/). (B) 2-photon micrograph showing the phagocytic populations of the lymph node based of the expression of the markers CD169

For Review Only

(red) and CX3R1 (green), SSM (CD169+, CX3CR1+), DC(CD169-, CX3CR1+), MM(CD169+, CX3CR1-). (C) Chitosan (CS) and inulin (INU) DiD-labeled NCs of two different sizes (S, ≈ 70 nm and M, 170 – 250 nm) were injected in the footpad of $CX_3CR_1^{+/gfp}$ and C57BL/6JRj mice (5 animals per group). After 12 hours, the PLNs from C57BL/6JRj were digested and the mean fluorescence intensity (MFI) evaluated by flow cytometry. (D) PLNs from $CX_3CR_1^{+/gfp}$ mice were evaluated using 2-photon microscopy (2PM). With this technique the MFI of each nanosytem in the medullar (Med) and the follicular (Fol) region was quantified. In E, a representative image of the PLNs. Upper row shows a maximum intensity projection of the whole z-stack of the lymph node, while lower row shows a slice with the different regions highlighted. SSM (CD169+) are shown in red, nanocapsules (NCs) in white, in blue the follicular DCs (CD21/35+) and in green cells of myeloid origin expressing CX_3CR_1 receptor. One-way ANOVA, Brown-Forsythe test. To simplify the interpretation, the comparisons were made only between the groups injected with NCs. The differences were considered significant for * $p < 0.05$, ** $p < 0.01$, *** $p < 0.001$ and **** $p < 0.0001$.

Figure 8. Interaction of the nanocapsules (NCs) the different subsets of immune cells in the popliteal lymph node (PLN). Chitosan (CS) and inulin (INU) NCs of two different sizes (S, ≈ 70 nm and M, 170 – 250 nm) were injected in the footpad of B6 mice (5 animals per group). After 12 hours the PLNs were collected, enzymatically digested and stained with an antibody panel specific to, macrophages (MHC II+, CD11b+, CD11c intlow, CD169+, and F4/80 positive in medullary macrophages, MM, and negative in subcapsular sinus macrophages, SSM) and dendritic cells (DC, MHC II+, CD11c+, CD11b positive or negative population). Percentage of DiD+ cells and the mean fluorescence intensity (MFI) are represented for each subset of immune cells. Analysis: all statistical analyses were performed assessing normal distribution of samples (Saphiro-Wilk test) and applying a one-way ANOVA test. * $p < 0.05$, ** $p < 0.01$, *** $p < 0.001$, **** $p < 0.0001$.

- **Table Legends**

Table 1. Different composition and preparation parameters of the nanosystems developed in this study.

Table 2. Physicochemical properties of the developed nanosystems. Particle size and PDI were obtained by dynamic light scattering. INU: inulin; CS: chitosan; NCs: nanocapsules; S: small size; M: medium size ($n \geq 10$).

Table 3. Cytokine secretion by iDCs after incubation with different nanocapsules (NCs).

- **Reference annotations**: authors should highlight 6–8 references that are of particular significance to the subject under discussion as **"* of interest"** or **"** of considerable interest"**, and provide a brief (1–2 line) synopsis.

For Review Only

References

1. Cordeiro AS, Alonso MJ, de la Fuente M. Nanoengineering of vaccines using natural polysaccharides. *Biotechnol. Adv.* [Internet]. 33(6), 1279–1293 (2015). Available from: http://linkinghub.elsevier.com/retrieve/pii/S0734975015300094.
2. Mensink MA, Frijlink HW, Van Der Voort Maarschalk K, Hinrichs WLJ. Inulin, a flexible oligosaccharide. II: Review of its pharmaceutical applications. *Carbohydr. Polym.* [Internet]. 134, 418–428 (2015). Available from: http://dx.doi.org/10.1016/j.carbpol.2015.08.022.
3. Skwarczynski M. Inulin: A New Adjuvant With Unknown Mode of Action. *EBioMedicine* [Internet]. 15, 8–9 (2017). Available from: http://dx.doi.org/10.1016/j.ebiom.2016.11.019.

*** Briefly describes the evidence on inulin adjuvant mechanism of action**

4. Silva DG, Cooper PD, Petrovsky N. Inulin-derived adjuvants efficiently promote both Th1 and Th2 immune responses. *Immunol. Cell Biol.* 82(6), 611–616 (2004).
5. Petrovsky N, Cooper PD. Advax™, a novel microcrystalline polysaccharide particle engineered from delta inulin, provides robust adjuvant potency together with tolerability and safety. *Vaccine* [Internet]. 33(44), 5920–5926 (2015). Available from: http://dx.doi.org/10.1016/j.vaccine.2015.09.030.
6. Wang L, Barclay T, Song Y, *et al.* Investigation of the biodistribution, breakdown and excretion of delta inulin adjuvant. *Vaccine* [Internet]. 35(34), 4382–4388 (2017). Available from: http://dx.doi.org/10.1016/j.vaccine.2017.06.045.
7. Stein J V., F. Gonzalez S. Dynamic intravital imaging of cell-cell interactions in the lymph node. *J. Allergy Clin. Immunol.* [Internet]. 139(1), 12–20 (2017). Available from: http://dx.doi.org/10.1016/j.jaci.2016.11.008.

***reviews the uses of 2-photon intravital microscopy and describes the different subsets of immune cells in the lymph nodes**

8. Jiang H, Wang Q, Sun X. Lymph node targeting strategies to improve vaccination efficacy. *J. Control. Release* [Internet]. 267(May), 47–56 (2017). Available from: https://doi.org/10.1016/j.jconrel.2017.08.009.

****Summarizes the critical factors that affect lymph node delivery**

9. Reddy ST, Swartz MA, Hubbell JA. Targeting dendritic cells with biomaterials: developing the next generation of vaccines. *Trends Immunol.* [Internet]. 27(12), 573–579 (2006). Available from: http://www.ncbi.nlm.nih.gov/pubmed/17049307.

****Points out the potential of improving vaccines by targeting antigen to the lymph nodes**

10. Moyer TJ, Zmolek AC, Irvine DJ. Beyond antigens and adjuvants: formulating future vaccines. *J. Clin. Invest.* 126(3), 799–808 (2016).
11. Benne N, van Duijn J, Kuiper J, Jiskoot W, Slütter B. Orchestrating immune responses: How size,

For Review Only

shape and rigidity affect the immunogenicity of particulate vaccines. *J. Control. Release* [Internet]. 234, 124–134 (2016). Available from: http://dx.doi.org/10.1016/j.jconrel.2016.05.033.

12. Zhu G, Zhang F, Ni Q, Niu G, Chen X. Efficient Nanovaccine Delivery in Cancer Immunotherapy. *ACS Nano*. 11(3), 2387–2392 (2017).
13. Gutjahr A, Phelip C, Coolen A-L, *et al.* Biodegradable Polymeric Nanoparticles-Based Vaccine Adjuvants for Lymph Nodes Targeting. *Vaccines 2016, Vol. 4, Page 34*. 4(4), 34 (2016).
14. Irvine DJ, Hanson MC, Rakhra K, Tokatlian T. Synthetic Nanoparticles for Vaccines and Immunotherapy. *Chem. Rev.* [Internet]. 115(19), 11109–11146 (2015). Available from: http://pubs.acs.org/doi/10.1021/acs.chemrev.5b00109.
15. Gause KT, Wheatley AK, Cui J, Yan Y, Kent SJ, Caruso F. Immunological Principles Guiding the Rational Design of Particles for Vaccine Delivery. *ACS Nano* [Internet]. 11(1), 54–68 (2017). Available from: http://pubs.acs.org/doi/10.1021/acsnano.6b07343.
16. An M, Li M, Xi J, Liu H. Silica Nanoparticle as a Lymph Node Targeting Platform for Vaccine Delivery. *ACS Appl. Mater. Interfaces*. 9(28), 23466–23475 (2017).
17. Almeida JPM, Lin AY, Figueroa ER, Foster AE, Drezek RA. In vivo gold nanoparticle delivery of peptide vaccine induces anti-tumor immune response in prophylactic and therapeutic tumor models. *Small*. 11(12), 1453–1459 (2015).
18. Zeng Q, Li H, Jiang H, *et al.* Tailoring polymeric hybrid micelles with lymph node targeting ability to improve the potency of cancer vaccines. *Biomaterials* [Internet]. 122, 105–113 (2017). Available from: http://dx.doi.org/10.1016/j.biomaterials.2017.01.010.
19. Reddy ST, Rehor A, Schmoekel HG, Hubbell JA, Swartz MA. In vivo targeting of dendritic cells in lymph nodes with poly(propylene sulfide) nanoparticles. *J. Control. Release*. 112(1), 26–34 (2006).
20. Manolova V, Flace A, Bauer M, Schwarz K, Saudan P, Bachmann MF. Nanoparticles target distinct dendritic cell populations according to their size. *Eur. J. Immunol.* [Internet]. 38(5), 1404–13 (2008). Available from: http://www.ncbi.nlm.nih.gov/pubmed/18389478.

****Describes the effect of the nanoparticle size in the access and biodistribution inside the lymph nodes**

21. Perrie Y, Crofts F, Devitt A, Griffiths HR, Kastner E, Nadella V. Designing liposomal adjuvants for the next generation of vaccines. *Adv. Drug Deliv. Rev.* 99, 85–96 (2016).
22. Rajput MKS, Kesharwani SS, Kumar S, Muley P, Narisetty S, Tummala H. Dendritic Cell-Targeted Nanovaccine Delivery System Prepared with an Immune-Active Polymer. *ACS Appl. Mater. Interfaces* [Internet]. 10(33), 27589–27602 (2018). Available from: http://pubs.acs.org/doi/10.1021/acsami.8b02019.
23. Calvo P, Remuñán-López C, Vila-Jato JL, Alonso MJ. Development of positively charged colloidal drug carriers: Chitosan-coated polyester nanocapsules and submicron-emulsions. *Colloid Polym. Sci.* [Internet]. 275(1), 46–53 (1997). Available from: http://dx.doi.org/10.1007/s003960050050.

For Review Only

24. Braun D. A two-step induction of indoleamine 2,3 dioxygenase (IDO) activity during dendritic-cell maturation. *Blood* [Internet]. 106(7), 2375–2381 (2005). Available from: http://www.bloodjournal.org/cgi/doi/10.1182/blood-2005-03-0979.

25. Jung S, Aliberti J, Graemmel P, *et al.* Analysis of Fractalkine Receptor CX3CR1 Function by Targeted Deletion and Green Fluorescent Protein Reporter Gene Insertion. *Mol. Cell. Biol.* [Internet]. 20(11), 4106–4114 (2000). Available from: http://mcb.asm.org/cgi/doi/10.1128/MCB.20.11.4106-4114.2000.

26. Crecente-Campo J, Alonso MJ. Engineering, on-demand manufacturing, and scaling-up of polymeric nanocapsules. *Bioeng. Transl. Med.* (2018).

***Describes how to prepare nanocapsules with particle size < 100 nm**

27. Crecente-Campo J, Lorenzo-Abalde S, Mora A, *et al.* Bilayer polymeric nanocapsules: A formulation approach for a thermostable and adjuvanted E. coli antigen vaccine. *J. Control. Release* [Internet]. 286, 20–32 (2018). Available from: https://www.sciencedirect.com/science/article/pii/S0168365918304127?via%3Dihub.

28. Lozano M V, Esteban H, Brea J, Loza MI, Torres D, Alonso MJ. Intracellular delivery of docetaxel using freeze-dried polysaccharide nanocapsules. *J. Microencapsul.* [Internet]. 30(2), 181–8 (2013). Available from: http://www.ncbi.nlm.nih.gov/pubmed/23088320.

29. Vicente S, Diaz-Freitas B, Peleteiro M, *et al.* A Polymer/Oil Based Nanovaccine as a Single-Dose Immunization Approach. *PLoS One* [Internet]. 8(4), e62500 (2013). Available from: http://dx.plos.org/10.1371/journal.pone.0062500.

30. Vicente S, Peleteiro M, González-Aramundiz JV, *et al.* Highly versatile immunostimulating nanocapsules for specific immune potentiation. *Nanomedicine (London)* [Internet]. 9, 2273–2289 (2014). Available from: http://www.ncbi.nlm.nih.gov/pubmed/24673264.

31. Moriguchi S, Kaneyasu M. Role of Vitamin E in Immune System. *Ser. Rev. J.Clin. Biochem.* [Internet]. 34, 97–109 (2003). Available from: https://www.jstage.jst.go.jp/article/jcbn1986/34/3/34_3_97/_pdf/-char/en.

32. Irvine DJ, Swartz MA, Szeto GL. Engineering synthetic vaccines using cues from natural immunity. *Nat. Mater.* [Internet]. 12(11), 978–990 (2013). Available from: http://dx.doi.org/10.1038/nmat3775.

33. Kim S-Y, Noh Y-W, Kang TH, *et al.* Synthetic vaccine nanoparticles target to lymph node triggering enhanced innate and adaptive antitumor immunity. *Biomaterials* [Internet]. 130, 56–66 (2017). Available from: http://dx.doi.org/10.1016/j.biomaterials.2017.03.034.

34. Vicente S, Peleteiro M, Díaz-Freitas B, Sanchez A, González-Fernández Á, Alonso MJ. Co-delivery of viral proteins and a TLR7 agonist from polysaccharide nanocapsules: A needle-free vaccination strategy. *J. Control. Release* [Internet]. 172(3), 773–781 (2013). Available from: http://dx.doi.org/10.1016/j.jconrel.2013.09.012.

35. Oyarzun-Ampuero FA, Garcia-Fuentes M, Torres D, Alonso MJ. Chitosan-coated lipid nanocarriers for therapeutic applications. *J. Drug Deliv. Sci. Technol.* [Internet]. 20(4), 259–265

For Review Only

(2010). Available from: http://linkinghub.elsevier.com/retrieve/pii/S1773224710500431.

36. Mellman I, Steinman RM. Dendritic Cells: Specialized and Regulated Antigen Processing Machines. *Cell* [Internet]. 106(3), 255–258 (2001). Available from: https://ac.els-cdn.com/S0092867401004494/1-s2.0-S0092867401004494-main.pdf?_tid=ad7a3c08-a962-4555-83ec-958a0ac4f57f&acdnat=1553004993_c450e1b643de143fd8b09d7d9bbcc842.

37. Fifis T, Gamvrellis A, Crimeen-Irwin B, *et al.* Size-Dependent Immunogenicity: Therapeutic and Protective Properties of Nano-Vaccines against Tumors. *J. Immunol.* [Internet]. 173(5), 3148–3154 (2004). Available from: http://www.ncbi.nlm.nih.gov/pubmed/15322175.

38. Foged C, Brodin B, Frokjaer S, Sundblad A. Particle size and surface charge affect particle uptake by human dendritic cells in an in vitro model. *Int. J. Pharm.* [Internet]. 298(2), 315–322 (2005). Available from: http://www.ncbi.nlm.nih.gov/pubmed/15961266.

39. Gamvrellis A, Leong D, Hanley JC, Xiang SDUED, Mottram P, Plebanski M. Vaccines that facilitate antigen entry into dendritic cells. *Immunol. Cell Biol.* 82(5), 506–516 (2004).

40. Fromen CA, Rahhal TB, Robbins GR, *et al.* Nanoparticle surface charge impacts distribution, uptake and lymph node trafficking by pulmonary antigen-presenting cells. *Nanomedicine Nanotechnology, Biol. Med.* [Internet]. 12(3), 677–687 (2016). Available from: http://dx.doi.org/10.1016/j.nano.2015.11.002.

41. Villiers C, Chevallet M, Diemer H, *et al.* From Secretome Analysis to Immunology. *Mol. Cell. Proteomics* [Internet]. 8(6), 1252–1264 (2009). Available from: http://www.mcponline.org/lookup/doi/10.1074/mcp.M800589-MCP200.

42. Koppolu B, Zaharoff DA. The effect of antigen encapsulation in chitosan particles on uptake, activation and presentation by antigen presenting cells. *Biomaterials* [Internet]. 34(9), 2359–2369 (2013). Available from: http://dx.doi.org/10.1016/j.biomaterials.2012.11.066.

43. Mellor AL, Lemos H, Huang L. Indoleamine 2,3-Dioxygenase and Tolerance: Where Are We Now? *Front. Immunol.* [Internet]. 8(OCT), 1–6 (2017). Available from: http://journal.frontiersin.org/article/10.3389/fimmu.2017.01360/full.

44. Durgeau A, Virk Y, Corgnac S, Mami-Chouaib F. Recent Advances in Targeting CD8 T-Cell Immunity for More Effective Cancer Immunotherapy. *Front. Immunol.* [Internet]. 9(JAN) (2018). Available from: http://journal.frontiersin.org/article/10.3389/fimmu.2018.00014/full.

45. Lam S, Bollard C. T-cell therapies for HIV. *Immunotherapy* [Internet]. 5(4), 407–414 (2013). Available from: https://www.futuremedicine.com/doi/10.2217/imt.13.23.

46. Slütter B, Jiskoot W. Sizing the optimal dimensions of a vaccine delivery system: a particulate matter. *Expert Opin. Drug Deliv.* [Internet]. 13(2), 167–170 (2016). Available from: http://www.tandfonline.com/doi/full/10.1517/17425247.2016.1121989.

47. Mottram PL, Leong D, Crimeen-Irwin B, *et al.* Type 1 and 2 Immunity Following Vaccination Is Influenced by Nanoparticle Size: Formulation of a Model Vaccine for Respiratory Syncytial Virus. *Mol. Pharm.* [Internet]. 4(1), 73–84 (2007). Available from: http://pubs.acs.org/doi/abs/10.1021/mp060096p.

For Review Only

48. Hirai T, Yoshioka Y, Takahashi H, *et al.* Amorphous silica nanoparticles enhance cross-presentation in murine dendritic cells. *Biochem. Biophys. Res. Commun.* [Internet]. 427(3), 553–556 (2012). Available from: http://linkinghub.elsevier.com/retrieve/pii/S0006291X12018426.

49. Jia L, Gao X, Wang Y, Yao N, Zhang X. Structural, phenotypic and functional maturation of bone marrow dendritic cells (BMDCs) induced by Chitosan (CTS). *Biologicals* [Internet]. 42(6), 334–338 (2014). Available from: http://dx.doi.org/10.1016/j.biologicals.2014.07.004.

50. Oliveira M, Santos S, Oliveira M, Torres A, Barbosa M. Chitosan drives anti-inflammatory macrophage polarisation and pro-inflammatory dendritic cell stimulation. *Eur. Cells Mater.* [Internet]. 24, 136–153 (2012). Available from: http://www.ecmjournal.org/journal/papers/vol024/pdf/v024a10.pdf.

51. Vogt L, Meyer D, Pullens G, *et al.* Immunological Properties of Inulin-Type Fructans. *Crit. Rev. Food Sci. Nutr.* [Internet]. 55(3), 414–436 (2015). Available from: http://www.tandfonline.com/doi/abs/10.1080/10408398.2012.656772.

52. Moran HBT, Turley JL, Andersson M, Lavelle EC. Immunomodulatory properties of chitosan polymers. *Biomaterials* [Internet]. 184(August), 1–9 (2018). Available from: https://doi.org/10.1016/j.biomaterials.2018.08.054.

53. Li L, Honda-Okubo Y, Li C, Sajkov D, Petrovsky N. Delta inulin adjuvant enhances plasmablast generation, expression of activation-induced cytidine deaminase and B-cell affinity maturation in human subjects receiving seasonal influenza vaccine. *PLoS One*. 10(7), 1–18 (2015).

54. Hayashi M, Aoshi T, Haseda Y, *et al.* Advax, a delta inulin microparticle, potentiates in-built adjuvant property of co-administered vaccines. *EBioMedicine* [Internet]. 15, 127–136 (2017). Available from: http://dx.doi.org/10.1016/j.ebiom.2016.11.015.

55. Tomar J, Patil HP, Bracho G, *et al.* Advax augments B and T cell responses upon influenza vaccination via the respiratory tract and enables complete protection of mice against lethal influenza virus challenge. *J. Control. Release* [Internet]. 288(June), 199–211 (2018). Available from: https://doi.org/10.1016/j.jconrel.2018.09.006.

***Proposes a mechanism of action for inulin as an adjuvant**

56. Swartz MA, Hubbell JA, Reddy ST. Lymphatic drainage function and its immunological implications: From dendritic cell homing to vaccine design. *Semin. Immunol.* [Internet]. 20(2), 147–156 (2008). Available from: http://linkinghub.elsevier.com/retrieve/pii/S1044532307001091.

57. Mueller SN, Tian S, DeSimone JM. Rapid and Persistent Delivery of Antigen by Lymph Node Targeting PRINT Nanoparticle Vaccine Carrier To Promote Humoral Immunity. *Mol. Pharm.* [Internet]. 12(5), 1356–1365 (2015). Available from: http://pubs.acs.org/doi/pdf/10.1021/mp500589c.

58. Cordeiro AS, Crecente-Campo J, Bouzo BL, González SF, de la Fuente M, Alonso MJ. Engineering polymeric nanocapsules for an efficient drainage and biodistribution in the lymphatic system. *J. Drug Target.* [Internet]. (just-accepted), 1–13 (2019). Available from:

For Review Only

https://doi.org/10.1080/1061186X.2018.1561886.

59. Ballou B, Andreko SK, Osuna-Highley E, *et al.* Nanoparticle Transport from Mouse Vagina to Adjacent Lymph Nodes. *PLoS One*. 7(12) (2012).

60. Park JH, Park J, Kim S, *et al.* Characterization and application of porous gold nanoparticles as 2-photon luminescence imaging agents: 20-fold brighter than gold nanorods. *J. Biophotonics*. 11(2), 1–7 (2018).

61. Bachmann MF, Jennings GT. Vaccine delivery: a matter of size, geometry, kinetics and molecular patterns. *Nat. Rev. Immunol.* [Internet]. 10(11), 787–796 (2010). Available from: http://dx.doi.org/10.1038/nri2868.

62. Pitorre M, Bastiat G, dit Chatel EM, Benoit J-P. Passive and specific targeting of lymph nodes: the influence of the administration route. *Eur. J. Nanomedicine* [Internet]. 7(2), 121–128 (2015). Available from: https://www.degruyter.com/view/j/ejnm.2015.7.issue-2/ejnm-2015-0003/ejnm-2015-0003.xml.

63. Gray EE, Cyster JG. Lymph Node Macrophages. *J. Innate Immun.* [Internet]. 4(5–6), 424–436 (2012). Available from: https://www.karger.com/Article/FullText/337007.

***Describes the different populations of macrophages in the lymph nodes and their functions**

64. Rincon-Restrepo M, Mayer A, Hauert S, *et al.* Vaccine nanocarriers: Coupling intracellular pathways and cellular biodistribution to control CD4 vs CD8 T cell responses. *Biomaterials* [Internet]. 132, 48–58 (2017). Available from: http://dx.doi.org/10.1016/j.biomaterials.2017.03.047.

65. Gonzalez SF, Lukacs-Kornek V, Kuligowski MP, *et al.* Capture of influenza by medullary dendritic cells via SIGN-R1 is essential for humoral immunity in draining lymph nodes. *Nat. Immunol.* [Internet]. 11(5), 427–434 (2010). Available from: http://dx.doi.org/10.1038/ni.1856.

66. Kuka M, Iannacone M. The role of lymph node sinus macrophages in host defense. *Ann. N. Y. Acad. Sci.* [Internet]. 1319(1), 38–46 (2014). Available from: http://doi.wiley.com/10.1111/nyas.12387.

67. Moran I, Grootveld AK, Nguyen A, Phan TG. Subcapsular Sinus Macrophages: The Seat of Innate and Adaptive Memory in Murine Lymph Nodes. *Trends Immunol.* [Internet]. 40(1), 35–48 (2019). Available from: https://linkinghub.elsevier.com/retrieve/pii/S1471490618302114.

68. Gonzalez SF, Degn SE, Pitcher LA, Woodruff M, Heesters BA, Carroll MC. Trafficking of B Cell Antigen in Lymph Nodes. *Annu. Rev. Immunol.* [Internet]. 29(1), 215–233 (2011). Available from: http://www.annualreviews.org/doi/10.1146/annurev-immunol-031210-101255.

69. Chatziandreou N, Farsakoglu Y, Palomino-Segura M, *et al.* Macrophage Death following Influenza Vaccination Initiates the Inflammatory Response that Promotes Dendritic Cell Function in the Draining Lymph Node. *Cell Rep.* [Internet]. 18(10), 2427–2440 (2017). Available from: http://dx.doi.org/10.1016/j.celrep.2017.02.026.

70. Gerner MY, Torabi-parizi P, Germain RN, Gerner MY, Torabi-parizi P, Germain RN. Strategically Localized Dendritic Cells Promote Rapid T Cell Responses to Lymph-Borne Particulate Article

For Review Only

Strategically Localized Dendritic Cells Promote Rapid T Cell Responses to Lymph-Borne Particulate Antigens. *Immunity* [Internet]. 42(1), 172–185 (2015). Available from: http://dx.doi.org/10.1016/j.immuni.2014.12.024.

71. Gasteiger G, Ataide M, Kastenmüller W. Lymph node - an organ for T-cell activation and pathogen defense. *Immunol. Rev.* [Internet]. 271(1), 200–220 (2016). Available from: http://doi.wiley.com/10.1111/imr.12399.

For Review Only

Supplementary information

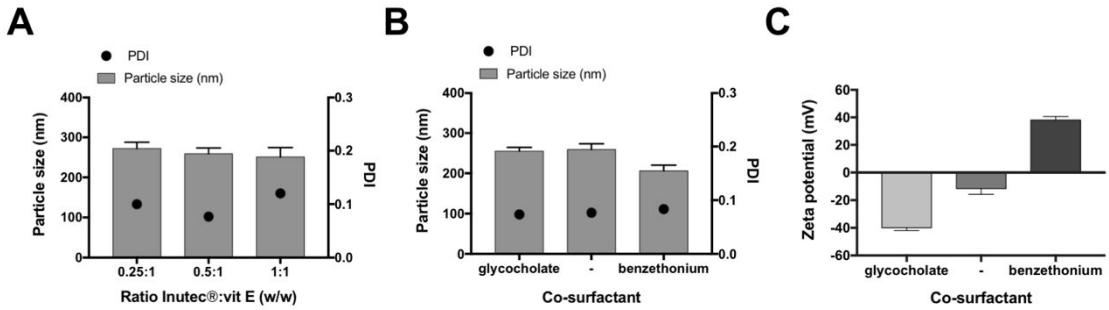

Figure S1. Influence of the ratio Inutec®:vitamin E (w/w) in the particle size of the resulting nanocapsules (A). The addition of a co-surfactant, such us sodium glycocholate or benzethonium chloride, rendered nanocapsules of similar particle size (B) but very different surface charge (C).

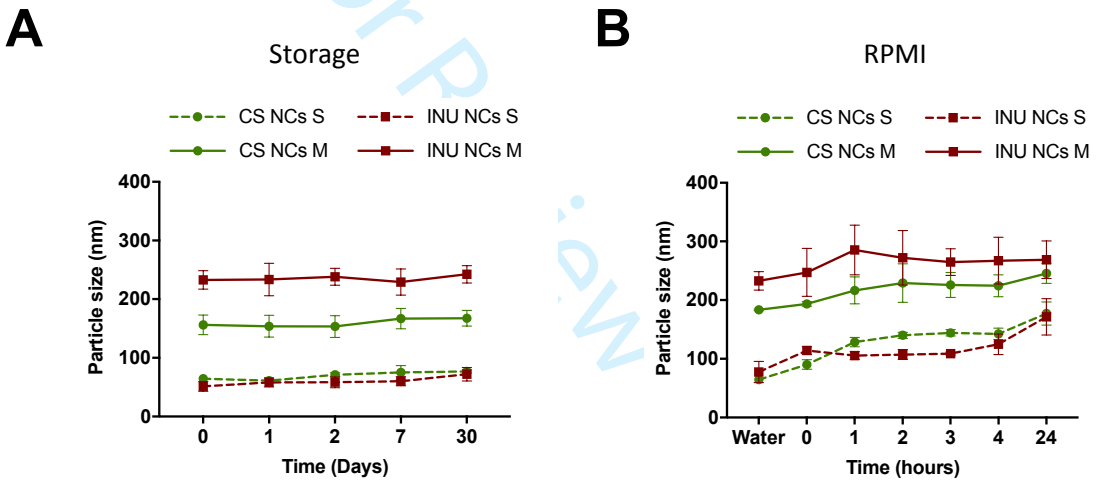

Figure S2. Stability of the nanosystems regarding their particle size in storage conditions at 4 ºC (A) and in cell culture medium at 37 ºC (B). Inulin-based nanocapsules (INU NCs) and chitosan nanocapsules (CS NCs) of two different sizes, small (S, ≈ 70 nm) and medium (M, 170 – 250 nm).

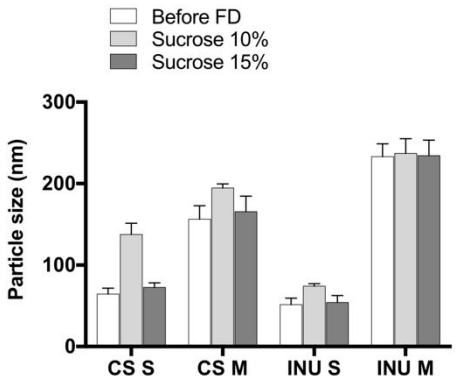

Figure S3. Stability of the freeze-dried formulations. To assure the long-term stability of the systems a freeze-drying process was optimized, using sucrose as cryoprotectant (B). CS: chitosan; INU: inulin; S: small size (≈ 70 nm), M: medium size (170 – 250 nm) nanocapsules; FD: freeze-drying.

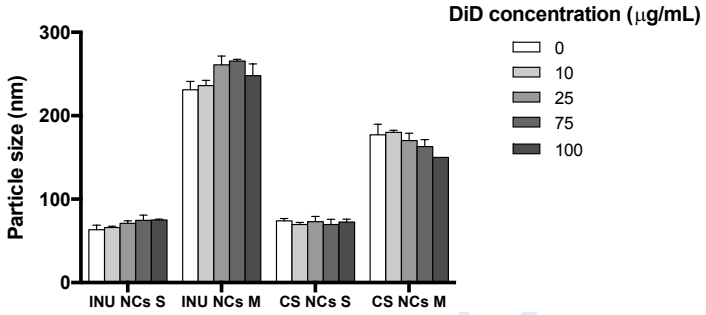

Figure S4. Influence of the fluorescent marker DiD concentration in the particle size of the different nanocapsules (NCs): inulin (INU) and chitosan (CS), small (S, ≈ 70 nm) and medium (M, 170 – 150 nm) size.